Acidification, deoxygenation, nutrient and biomasses decline in a warming Mediterranean Sea

Marco Reale[1], Gianpiero Cossarini[1], Paolo Lazzari[1], Tomas Lovato[2], Giorgio Bolzon[1], Simona Masina[2], Cosimo Solidoro[1], Stefano Salon[1]

1. National Institute of Oceanography and Applied Geophysics - OGS, Trieste, Italy
2. Fondazione Centro Euro-Mediterraneo sui Cambiamenti Climatici, CMCC, Ocean Modeling and Data Assimilation Division, Bologna, Italy

Correspondence to: Marco Reale (mreale@inogs.it) and Stefano Salon (ssalon@inogs.it)

Abstract. The projected warming, nutrient decline, changes in net primary production, deoxygenation and acidification of the global ocean will affect marine ecosystems during the 21st century. Here the climate change-related impacts in the marine ecosystems of the Mediterranean Sea in the middle and at the end of the 21st century are assessed using high-resolution projections of the physical and biogeochemical state of the basin under the Representative Concentration Pathways (RCPs) 4.5 and 8.5. The analysis shows in both scenarios changes in the dissolved nutrient content of the euphotic and intermediate layers of the basin, net primary production, phytoplankton respiration and carbon stock (including phytoplankton, zooplankton, bacterial biomass and particulate organic matter). The projections also show a uniform surface and subsurface reduction in the oxygen concentration driven by the warming of the water column and by the increase in ecosystem respiration, and an acidification signal in the upper water column, linked to the increase in the dissolved inorganic carbon content of the water column due to CO_2 absorption from the atmosphere and the increase in respiration. The projected changes are stronger in the RCP8.5 (worst-case) scenario and, in particular, in the Eastern Mediterranean due to the limited influence of the exchanges in the Strait of Gibraltar in that part of the basin. On the other hand, the analysis of the projections under RCP4.5 emission scenario shows a tendency to recover the values observed at the beginning of the 21st century for several biogeochemical variables in the second half of the period. This result supports the idea - possibly based on the existence, in a system like the Mediterranean Sea, of a certain buffer capacity and renewal rate - that the implementation of policies of reducing CO_2 emission could be, indeed, effective and could contribute to the foundation of ocean sustainability science and policies.

1. Introduction

The Mediterranean Sea (Fig. 1) is a mid-latitude semi-enclosed basin surrounded by the continental areas of Southern Europe, Northern Africa and the Middle East. The basin is characterized by a thermohaline circulation composed of three distinctive cells. The first is an open cell associated with the inflow of the Atlantic Water (AW) at the Strait of Gibraltar (which undergoes a progressive increase in salinity due to evaporation becoming Modified Atlantic Water, or MAW) and the formation of Levantine Intermediate Water (LIW) in the Eastern basin (Lascaratos, 1993; Nittis and Lascaratos, 1998; Velaoras et al., 2019; Fach et al., 2021; Fedele et al., 2021). The other two are closed cells associated with deep water

formation processes occurring in the Gulf of Lion (located in the North Western Mediterranean, Fig.1; Somot et al., 2018 and reference therein) and in the Adriatic Sea (Fig. 1; Mantziafou and Lascaratos 2004, 2008; Schroeder et al., 2012 and references therein).

Future climate projections for the Mediterranean region based on different emission scenarios show, at the end of the 21st century, (i) a reduction in precipitation and a general warming of the area (e.g., Giorgi, 2006; Diffenbaugh et al., 2007; Giorgi and Lionello, 2008; Dubois et al., 2012; Lionello et al., 2012; Planton et al., 2012; Gualdi et al., 2013; MedEEC, 2020), (ii) a warming of seawater (Somot et al., 2006; Adloff et al., 2015; Soto-Navarro et al., 2020; MedECC, 2020), and (iii) a consistent weakening of the thermohaline circulation and an increase in the stratification index throughout the basin (Somot et al., 2006; Adloff et al., 2015; Soto-Navarro et al., 2020) and a further increase in frequency and severity of atmospheric and marine heat waves and drought (Galli et al., 2017; Darmaraki et al., 2019; Ibrahim et al., 2021; Mathbout et al., 2021). Conversely, the future evolution of sea surface salinity in the Mediterranean Sea and the sign of its change are still uncertain due to the role played by rivers and Strait of Gibraltar exchanges (Adloff et al., 2015; Soto-Navarro et al., 2020; MedECC, 2020). In general, the magnitude of the projected changes has been shown to be dependent on the adopted emission scenario (MedECC, 2020).
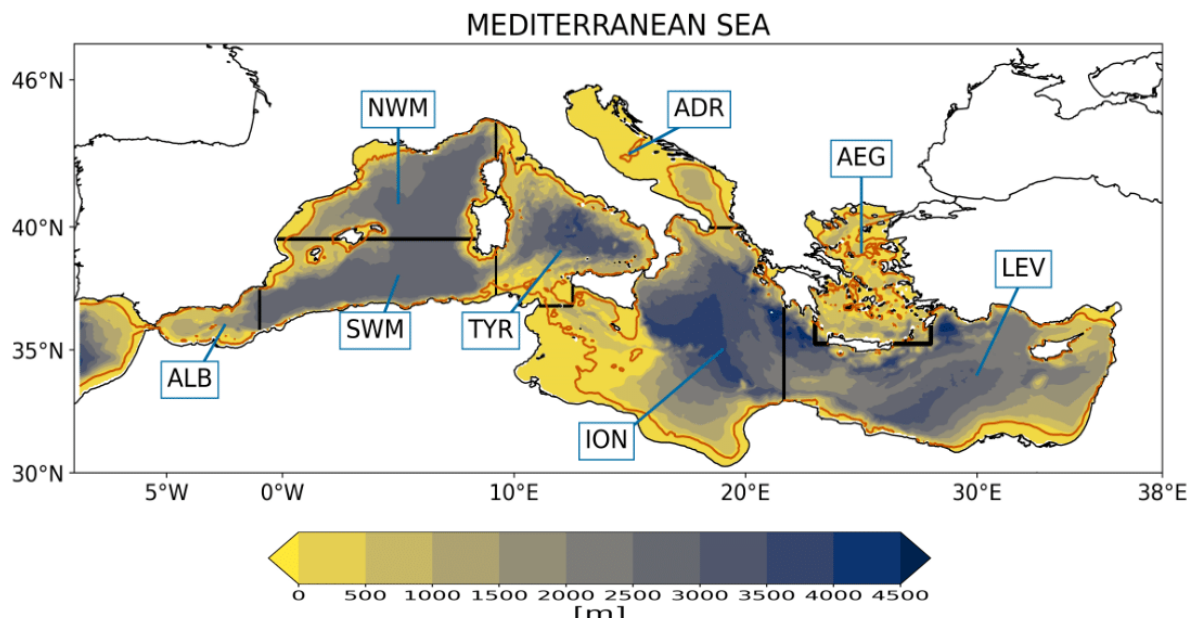
Fig.1 Mediterranean Sea bathymetry (in m) and relative sub-basins considered in the analysis: Alboran Sea (ALB), North Western Mediterranean (NWM), South Western Mediterranean (SWM), Tyrrhenian (TYR), Adriatic Sea (ADR), Ionian Sea (ION), Aegean Sea (AEG), Levantine basin (LEV). The dark orange line marks the 200 m isobath in the model domain. The domain boundary is set at longitude 8.8°W, westward of the Strait of Gibraltar.

From a biogeochemical point of view, the Mediterranean Sea is considered as an oligotrophic (ultraoligotrophic in its Eastern part) basin (Bethoux et al., 1998; Moutin and Raimbault, 2002; Siokou-Frangou et al., 2010; Lazzari et al., 2012). It is characterized by low productivity levels and an east-west trophic gradient (Crise et al.,1999; D'Ortenzio and Ribera d'Alcala 2009; Lazzari et al., 2012) which results from the superposition of different mechanisms such as the biological pump, the estuarine inverse circulation, and the position of nitrate (NO_3) and phosphate (PO_4) sources (Crise et al., 1999; Crispi et al., 2001). The only exceptions to the oligotrophy of the basin are some areas (Gulf of Lion, Strait of Sicily,

Algerian coastlines, Southern Adriatic Sea, Ionian Sea, Aegean Sea and Rhodes Gyre) where strong vertical mixing and upwelling phenomena associated with air-sea interactions and wind stress forcing enrich the surface in nutrients, so favouring phytoplankton rapid growth (or bloom) mostly in the late winter-early spring period (D'Ortenzio and Ribera d'Alcala, 2009; Reale et al., 2020b). A proxy widely adopted to detect phytoplankton blooms is the surface concentration of chlorophyll-*a* (chl-*a)* that is characterized by relative high values in specific open sea/coastal areas, where it is linked to the physical forcing and river inflow (D'Ortenzio and Ribera d'Alcala, 2009; Lazzari et al., 2012; Herrmann et al., 2013; Auger et al., 2014; Richon et al., 2018; Di Biagio et al., 2019; Reale et al., 2020a). The open sea chl-*a* vertical dynamics follows a seasonal cycle with winter-early spring surface blooms, and summer onset of a deep chl-*a* maximum (DCM) which deepens from approximately 50 m in the Western areas to 100 m in the Eastern areas (e.g. Lazzari et al., 2012; Macias et al., 2014; Lavigne et al., 2015; Cossarini et al., 2021).

Due to the strong links between ocean/atmosphere dynamics and biogeochemical patterns, it has to be expected that future climate change will have relevant impacts on the biogeochemistry and, in turn, on the marine ecosystem dynamics of the Mediterranean Sea. In fact, all the projected changes for the region will likely affect the vertical mixing and reduce the nutrient supply into the euphotic layer of the Mediterranean Sea (e.g. Richon et al., 2019), which is essential for phytoplankton dynamics and productivity, with possible impacts on the biogeochemical carbon cycle and carbon dioxide (CO_2)exchange with the atmosphere (e.g., Lazzari et al., 2012; Cossarini et al., 2015; Canu et al., 2015; Solidoro et al., 2022).

An assessment of the effects of climate change on the biogeochemistry and marine ecosystem dynamics of the Mediterranean Sea has been considered in a number of previous studies based on different emission scenarios. Hermann et al. (2014) assessed the response of the pelagic planktonic ecosystem of the North Western Mediterranean to different emission scenarios and showed that, at end of the 21st century, the biogeochemical processes and marine ecosystem components should be very similar to those observed at the end of the 20th century, although quantitative differences might be observed, such as an increase in the bacteria growth, gross primary production and biomass of small-size phytoplankton group. Lazzari et al. (2014) found a negative change in the plankton biomass in response to the A1B emission scenario, resulting from an increase of productivity and community respiration. Benedetti et al. (2018), using environmental niche models and considering six physical simulations based on different emission scenarios (A2, A2-F, A2-RF, A2-ARF, A1B-ARF, B1-ARF; Adloff et al., 2015), projected, in response to climate change, a loss of copepods diversity throughout most of the surface layer of the Mediterranean Sea. On the other hand, Moullec et al. (2019) under RCP8.5 emission scenario found an increase/decrease in both phytoplankton biomass and net primary production by the end of the 21st century in the Eastern/Western Mediterranean Sea. Macias et al. (2015) showed that, under emission scenarios RCP4.5 and RCP8.5 and despite a significant observed warming trend, the mean integrated primary production rate in the entire basin will remain almost unchanged in the 21st century. However, they pointed out some peculiar spatial differences in the basin such as an increase in the oligotrophy of the Western basin due to a surface density decrease and an increase in net primary production in the Eastern basin due to the increased density. Richon et al. (2019) observed, under the A2 emission scenario (which is similar to the RCP8.5 emission scenario in terms of magnitude of the projected changes in the global mean temperature), an accumulation of nitrate in the basin and a reduction of 10% in net primary productivity by 2090, with a peak of 50% in specific areas (including the Aegean Sea). On the other hand, no tendencies in the phosphorus were observed. Pagès et al. (2020) showed, under emission scenario RCP8.5, a decline in the nutrient

concentration (stronger in NO_3 than PO_4) at the surface of the basin due to the increase in the vertical stratification and pointed out that the Mediterranean Sea will become less productive (14% decrease in integrated primary production in both Western and Eastern basins) and will be characterized by a reduction (22% in the Western basin and 38% in the Eastern basin) in large phytoplankton species abundance in favor of small organisms. All these changes will mainly affect the Western basin, while the Eastern basin will be less impacted (Pagès et al., 2020). Solidoro et al. (2022) discussed the evolution of the carbon cycling, budgets and fluxes of the basin under the A2 scenario, highlighting an increase in the trophodynamic carbon fluxes and showing, at the same time, that the increment in the plankton primary production will be more than compensated by the increase in the ecosystem total respiration, which corresponds to a decrease of the total living carbon and oxygen in the epipelagic layer. Moreover, Solidoro et al., (2022) also projected an increase of dissolved inorganic carbon (DIC) pool and quantified for the first time the related acidification of the basin, a process that might significantly alter the Mediterranean ecosystems (Zunino et al., 2017; 2019) and their capability to sustain ecosystem services (Zunino et al., 2021).

All the above-mentioned works demonstrate that the dynamics of the marine ecosystem may be affected directly and indirectly by climate change and the magnitude of their response is dependent on the emission scenario adopted. Different levels of warming, acidification and changes in the vertical distribution of the oxygen, nutrient concentration and net primary production related to water column stratification are all potential marine stressors affecting marine organisms and ecosystem dynamics (see Kwiatkowski et al., 2020 for a review about the synergistic effects among potential marine stressors).

A proper simulation of these marine stressors and related impacts require the adoption of suitable horizontal and vertical resolutions. In fact, it has been shown that meso and submesoscale structures of the Mediterranean circulation influence indeed the biogeochemical dynamics of many areas of the basin (Moutin and Prieur, 2012; Richon et al., 2019), while the vertical resolution affects the features of the simulated stratification and subsurface ventilation pathways (see Kwiatkowski et al., 2020 and reference therein for a review).

These considerations emphasize the importance of providing eddy-resolving future projections of the Mediterranean Sea biogeochemistry under different emission scenarios. In fact, although observational and modeling studies have been already carried out in the recent period to assess the importance of the mesoscale dynamics on the physical and biogeochemical state of limited areas of the Mediterranean Sea (e.g. Hermann et al., 2008; Moutin and Prieur, 2012; Guyennon et al., 2015; Ramirez-Romero et al., 2020), long-term eddy-resolving biogeochemical projections under different emission scenarios, to the best of the authors' knowledge, have not been analyzed so far in the region. Such projections might be used in future studies specifically focused on the analysis of climate change impact on specific organisms, habitats and/or local areas.

Therefore, here climate change-related impacts in the marine ecosystems of the Mediterranean Sea in the middle and at the end of the 21st century are assessed using eddy-resolving projections of the physical and biogeochemical state of the basin under emission scenarios RCP4.5 and RCP8.5. These projections are derived from the offline coupling between the physical model MFS16 (Mediterranean Forecasting System at 1/16º; Oddo et al., 2009) and the transport-reaction model OGSTM-BFM (OGS Transport Model-Biogeochemical Flux Model; Lazzari et al., 2012). The analysis focuses on 21st

century projected changes of dissolved nutrients and oxygen, net primary production, respiration, living/non-living organic matter, plankton and bacterial biomass, and particulate organic matter (POC). Moreover, the response of the basin to the increasing atmospheric CO_2 concentrations is thoroughly investigated. The projected changes are also correlated with changes in the physical forcing in the region.

The article is organized as follows: the MFS16-OGSTM-BFM system along with the physical forcing used to drive the biogeochemical scenarios, initial and boundary conditions and numerical experiments are described in Section 2. Section 3 discusses the projected changes in climate change-related impacts in the marine ecosystems of the Mediterranean basin. Finally, Section 4 summarizes and discusses the results of this work, together with their uncertainties, paving the way for possible future research avenues.

1. Data and Methods

The biogeochemical projections of the Mediterranean Sea state during the 21st century have been produced by driving the transport-reaction model OGSTM-BFM (Lazzari et al., 2012) with the 3D outputs of the physical model MFS16 (Oddo et al., 2009) through an off-line coupling. In fact, the physical model MFS16 supplies to the OGSTM-BFM the temporal evolution of daily horizontal and vertical current velocities, vertical eddy diffusivity, potential temperature, salinity, and surface data for solar shortwave irradiance and wind stress. The resulting transport processes affecting the concentration of biogeochemical tracers (advection, vertical diffusion and sinking) are computed by OGSTM, which is a modified version of the OPA tracer model (Océan PArallélisé, Foujols et al., 2000). The temporal evolution of biogeochemical processes is computed by the Biogeochemical Flux Model (BFM; Vichi et al., 2015).

2.1. The MFS16 physical model

MFS16 is the Mediterranean configuration of the NEMO modelling system (Nucleus for European Modelling of the Ocean; Madec, 2008; see also http://www.nemo-ocean.eu, version 3.4) and constitutes the climate implementation of the Mediterranean Ocean Forecasting System (Oddo et al., 2009; Lovato et al., 2013).

The original MFS16 domain covers the whole Mediterranean Sea and part of the neighboring Atlantic Ocean region with a horizontal grid resolution of 1/16° (~6.5 km) and 72 unevenly spaced vertical levels (ranging from 3 m at the surface down to 600 m in the deeper layers, see Lovato et al., 2013). The model computes the air-sea fluxes of water, momentum and heat using specific bulk formulae tuned for the Mediterranean Sea (Oddo et al., 2009) applied to the atmospheric fields obtained from the atmosphere-ocean general circulation model CMCC-CM (CMCC-Coupled model; Scoccimarro et al., 2011).

The open boundary conditions in the Atlantic region for the physical variables (zonal/meridional component of current velocity, sea surface height, temperature and salinity) were derived from the ocean component of the CMCC-CM coupled model, while the riverine freshwater discharges and fluxes in the Dardanelles Strait were provided by the hydrological component of the same coupled model (Gualdi et al., 2013). The initial conditions of the Mediterranean Sea were obtained from the gridded temperature and salinity data produced by the SeaDataNet infrastructure (http://www.seadatanet.org/).

186   The model was initially spun-up for 25 years under present climate conditions and then scenario simulations were
187   performed over the 2005-2100 period.
188
189   **2.2. The OGSTM-BFM transport-reaction model**
190
191   The OGSTM-BFM transport-reaction model is based on the coupling of a transport model (OGSTM) based on the OPA
192   system (Foujols et al., 2000) and the BFM biogeochemical reactor. OGSTM-BFM is fully described in Lazzari et al.
193   (2012, 2016), where it was used to simulate chl-*a*, primary production and nutrient dynamics of the Mediterranean Sea
194   for the 1998-2004 period.
195
196   The OGSTM transport model resolves the advection, vertical diffusion and the sinking terms of the biogeochemical
197   tracers. The temporal scheme of OGSTM is an explicit forward temporal scheme for the advection and horizontal
198   diffusion terms, whereas an implicit time scheme is adopted for the vertical diffusion. The BFM biogeochemical reactor
199   considers co-occurring effects of multi-nutrient interactions and energy/material fluxes through the classical food chain
200   and the microbial food web which are both very important in the Mediterranean Sea (Bethoux et al., 1998). BFM has
201   been extensively applied to the studies of the dynamics of dissolved nutrients, chl-*a* and net primary production in the
202   Mediterranean Sea (Lazzari et al., 2012; 2016; Di Biagio et al., 2019; Reale et al., 2020a), marine carbon sequestration
203   and alkalinity (Canu et al., 2015; Cossarini et al., 2015; Butenschön et al., 2021), impacts of climate change on the
204   biogeochemical dynamics of marine ecosystems (Lazzari et al., 2014; Lamon et al., 2014; Solidoro et al., 2022), influence
205   of large-scale atmospheric circulation patterns on nutrient dynamics (Reale et al., 2020b) and operational short-term
206   forecasts for the Mediterranean Sea biogeochemistry (Teruzzi et al. 2018; 2019; Salon et al., 2019). The version adopted
207   here is the v5.
208
209   The model simulates the biogeochemical cycles of carbon, nitrogen, phosphorus and silicon through dissolved forms and
210   living organic and non-living organic compartments (labile, semi-labile and semi-refractory organic matter). Moreover,
211   it presently includes nine plankton functional types (PFTs), meant to be representative of diatoms, flagellates,
212   picophytoplankton, dinoflagellates, carnivorous and omnivorous mesozooplankton, bacteria, heterotrophic
213   nanoflagellates and microzooplankton. It also simulates the carbonate system dynamics, by solving the set of physico-
214   chemical equilibria related to total alkalinity (ALK) and dissolved inorganic carbon (DIC) chemical reactions (Cossarini
215   et al., 2015). ALK variability is driven by processes that alter the ion concentration in seawater (nitrification,
216   denitrification, uptake and release of nitrate, ammonia and phosphate by plankton cells, and precipitation and dissolution
217   of carbonate calcium-$CaCO_3$, see Wolf-Gladrow et al., 2007). DIC dynamics are driven by biological processes
218   (photosynthesis and respiration, precipitation and dissolution of $CaCO_3$) and physical processes (CO_2 exchanges at the
219   air-sea interface and, as for all the other biogeochemical tracers, dilution-concentration due to evaporation minus
220   precipitation processes).
221
222   **2.3. Initial and boundary conditions for the biogeochemistry**
223
224   Boundary conditions are adopted to represent the external supply of biogeochemical tracers and properties from the Strait
225   of Gibraltar and the rivers into the Mediterranean basin. The exchanges of nutrients and other biogeochemical tracers in

226   the Strait of Gibraltar are achieved by relaxing the 3D fields in the Atlantic zone (Fig. 1) to average vertical profiles
227   which, for dissolved oxygen, phosphate, nitrate and silicate, refer to Salon et al. (2019), while ALK is based on what was
228   described in Cossarini et al. (2015). These profiles do not consider a seasonal cycle or a future temporal evolution, with
229   DIC as the only exception, which is prescribed from a global ocean-climate simulation under RCP8.5 emission scenario
230   performed within the framework of the CMIP5 project (Coupled Model Intercomparison Project Phase 5; Taylor et al.,
231   2012) and based on the CMCC-CESM modeling system (CMCC-Coupled Earth System Model; Vichi et al., 2011). The
232   reasons for these choices rely on: (i) anomalous values observed in N:P ratio under the RCP8.5 emission scenario, (ii)
233   negligible variation, under emission scenario RCP8.5, of ALK along the 21st century, (iii) lack of a consistent RCP4.5
234   scenario, (iv) the possibility, using the same conditions at the Atlantic boundary, to test the impacts of the different
235   atmospheric and ocean forcings. Riverine inputs of phosphate, nitrate, dissolved oxygen, ALK and DIC are based on the
236   PERSEUS FP7-287600 project dataset (Policy-oriented marine environmental research in the Southern European seas;
237   Van Apeldoorn and Bouwman, 2014) and, also in this case, do not include temporal evolution in the future scenarios.

239   As observed in previous works (e.g. Richon et al., 2019), a transient scenario for the evolution of the atmospheric
240   deposition of nitrogen and phosphorus over the Mediterranean Sea is presently not available. Following Di Biagio et al.
241   (2019) and Reale et al. (2020a), the atmospheric deposition of phosphate and nitrate is parametrized as a mass flux at the
242   surface and is set for the entire basin equal to 4780 Mmol year^{-1} for phosphate and 81275 Mmol year^{-1} for nitrate.
243   Additional boundary conditions consider the sequestration of inorganic compounds in the marine sediment at the seabed.

245   The Representative Concentration Pathway (RCP) 4.5 and 8.5 emission scenarios (Moss et al., 2010) were used to force
246   the coupled physical-biogeochemical MFS16-OGSTM-BFM system. RCP4.5 represents an intermediate scenario in
247   which CO_2 emissions peak around 2040 (causing the maximum increase in CO_2 concentration), and then decline (with a
248   resulting CO_2 concentration plateau) while the RCP8.5 represents the worst-case scenario, in which CO_2 emissions
249   (eventually driven by feedback effects such as the release of greenhouse gasses from the permafrost) will continue to
250   increase throughout the 21st century, and the pCO_2 concentration will rise to more than 1200 ppm at the end of the 21st
251   century (IPCC, 2014). Recently some Authors have begun to consider the RCP8.5 scenario as "implausible", being based,
252   for example, on a large use of coal, larger than its effective availability at the end of 21st century (e.g. Hausfather and
253   Peters, 2020). On the other hand, it is still widely used to assess in the Mediterranean region the potential risks (also in
254   the marine ecosystems) emerging in an extreme warm world climate (5 °C) with respect to the pre-industrial era (IPCC,
255   2014). Because of that the projections under this emission scenario are still discussed here.

257   The initial conditions for the dissolved oxygen, nutrient, silicate and carbonate system variables are based on Medar-
258   Medatlas dataset (Mediterranean Data Archeology and Rescue-Mediterranean Atlas), as described in Cossarini et al.
259   (2015) and Salon et al. (2019).

260   Finally, all the simulations discussed in the next sections, use as initial conditions the resulting final fields from a run that
261   started in January, 1st 2005 following a spin-up of 100 years made with a loop over the 2005–2014 period for the physical
262   forcing, the river nutrient discharge and atmospheric forcing (nutrient deposition and CO_2 air value).

265   **2.4. Simulations protocol and set-up**

266

Long-term simulations can be affected by drifts in state variables due to the imbalance among boundary conditions, transport processes and internal element cycle formulations of the biogeochemical model. Therefore, a specific simulation protocol, based on the use of a control/scenario pair of simulation, has been implemented in order to disentangle the climate change signal from spurious signals (Solidoro et al., 2022). The protocol consists of a control simulation (CTRL) of 95 years and two 95-year biogeochemical scenario simulations, RCP4.5 and RCP8.5 (Fig.S1). All the simulations adopt as initial conditions the resulting final fields from the spin-up simulation (section 2.3). The CTRL is performed by repeating the 2005–2014 physical forcing and river discharge over the remaining 2015-2100 period (Fig. S1). The difference between each biogeochemical scenario and the CTRL provides the future evolution of a biogeochemical variable due to climate forcing.

Under each specific emission scenario and in the CTRL, our simulation protocol computes the time series of the mean annual 3D fields of the following variables: dissolved nutrients and oxygen, chl-a, net primary production, phytoplankton respiration, organic matter, plankton and bacterial biomass, POC, DIC and pH.

First, the annual 3D fields are vertically averaged over two separate key vertical levels: the surface zone and the intermediate zone. The first one spans the upper 100 m of the water column, which represents the location of MAW and the euphotic layer of the basin where most biological activities are concentrated. The second one covers the 200-600 m level, which includes the location of LIW. Only for the net primary production and phytoplankton respiration, a vertical integral over the 0-200 m layer is considered (Lazzari et al., 2012).

Second, the temporal evolution of the unbiased scenario starting from the present state, $U(k)_{SCEN}$ (with k = 2005, ..., 2099), is defined as:

$$U(k)_{SCEN} = X'_{SCEN} + X(k)_{SCEN} - X(k)_{CTRL} \qquad (1)$$

where X'_{SCEN} is the average of $X(k)_{SCEN}$ over the 2005-2020 period (hereafter the PRESENT, Fig.S1), and $X(k)_{SCEN}$ and $X(k)_{CTRL}$ are the yearly average in the scenario and CTRL simulations, respectively. We introduce the concept of "unbiased scenario" because equation (1) removes the effect of potential model drifts due to unbalanced boundary conditions and model errors. The time series of CTRL are filtered with a linear regression to keep the long-term drift and remove spurious variability. The period 2005-2020 has been chosen as reference (also in the forthcoming validation) due to: (i) the availability, after year 2000, of more advanced satellite and assimilated datasets to evaluate the biogeochemistry of the basin, (ii) to avoid the overlapping between historical and scenario part of the simulations (with the latter starting in 2005). It is important to stress here that the choice of the period should not significantly affect the results of the study as the observed differences during this period between the two scenarios for temperature, salinity and current speed fields have been found to be not statistically significant over most of the basin (not shown).

Finally, the temporal evolution of the climate change signal (CCS) with respect to the present is given by:

$$CCS(k)_{SCEN} = U(k)_{SCEN} - U_{SCEN-PRESENT} \qquad (2)$$

where $U_{SCEN-PRESENT}$ is the average of $U(k)_{SCEN}$ in the PRESENT. Hereafter, if not differently specified, all the shown time series will be represented by CCS_{SCEN}.

Horizontal spatial averages are computed considering the sub-basins defined in Fig. 1, the whole Mediterranean basin scale, and two macro-areas: the Western Mediterranean (WMED which includes ALB, SWM, NWM, TYR) and the Eastern Mediterranean (EMED which includes ION and LEV). The Adriatic and Aegean Seas are usually not considered part of the Eastern Mediterranean due to the importance of local forcing, such as riverine loads, in shaping the variability of the biogeochemical dynamics in those two sub-basins. Because of that, following the approach already adopted in previous works (Lazzari et al., 2012; 2016; Di Biagio et al., 2019; Reale et al., 2020 a,b) they are not considered in the spatial averages related to WMED and EMED.

Temporal averages of the climate change signals are computed over two 20-year periods: 2040-2059, hereafter referred to as "MID-FUTURE" and 2080-2099, hereafter referred to as "FAR-FUTURE" (Fig.S1). The relative climate change signals (in %, except for pH which will be measured in units of pH) in the MID-FUTURE or FAR-FUTURE periods with respect to the PRESENT are computed as:

$$U_{MID-FUTURE}=100*(U_{SCEN-MID-FUTURE}-U_{SCEN-PRESENT})/U_{SCEN-PRESENT} \quad (3)$$
$$U_{FAR-FUTURE}=100*(U_{SCEN-FAR-FUTURE}- U_{SCEN-PRESENT})/U_{SCEN-PRESENT} \quad (4)$$

where $U_{SCEN-MID-FUTURE}$, $U_{SCEN-FAR-FUTURE}$ and $U_{SCEN-PRESENT}$ are the averages of $U(k)_{SCEN}$ for the MID-FUTURE, FAR-FUTURE and PRESENT periods, respectively. Hereafter, if not differently specified, all the percentages shown in the maps are represented by $U_{MID-FUTURE}$ and $U_{FAR-FUTURE}$. The statistical significance of the relative climate change signals in each point of the basin is assessed by means of Mann-Whitney test with $p<0.05$.

3. Results

3.1 Evaluation of the MFS16-OGSTM-BFM control simulation for the present climate

MFS16 modelling system performances under present climate conditions were previously analyzed (Lovato et al., 2013; Galli et al., 2017), showing that the main spatio-temporal characteristics of the Mediterranean Sea physical properties reliably compared against ocean reanalysis datasets. Moreover, the physical reanalysis dataset produced by MFS16 within the Copernicus Marine Environmental Marine Service (CMEMS, Simoncelli et al., 2019) has already been coupled to the transport-reaction model OGSTM-BFM to carry out a reanalysis for the Mediterranean Sea biogeochemistry (Teruzzi et al., 2019). The latter is a biogeochemical dataset covering the 1999-2015 period at 1/16º resolution, which was already used for validating different biogeochemical simulations in the Mediterranean Sea, such as those based on MEDMIT12-BFM (Mediterranean MIT General circulation Model-BFM at 1/12º; Di Biagio et al., 2019) and RegCM-ES (Regional Climate Model-Earth System; Reale et al., 2020a) modelling systems. This dataset has been recently upgraded, refining the resolution to 1/24º and extending the period to 2019 (Teruzzi et al., 2021; Cossarini et al., 2021).

To date, no future climate biogeochemical projection of the Mediterranean Sea has been performed through this offline coupling.

345 Figure 2 a,b shows the surface average chl-*a* concentrations (upper 10 m) from the CTRL run compared with a
346 climatology based on satellite data available from CMEMS which covers the period 1999-2015 (Colella et al., 2016). The
347 model correctly reproduces the areas in the Mediterranean region characterized by relatively high values of chl-*a*: the
348 Alboran Sea, the Gulf of Lion, the coastal areas of the Adriatic Sea, and the Strait of Sicily. Moreover, the CTRL
349 simulation captures the west-east trophic gradient of chl-*a*, whose existence has been pointed out in previous works
350 (D'Ortenzio and Ribera d'Alcala, 2003; Lazzari et al., 2012; Colella et al., 2016; Richon et al., 2019; Di Biagio et al.
351 2019; Reale et al., 2020a). On the other hand, a general underestimation of approximately 50% of the chl-*a* signal
352 throughout the basin and in the coastal areas is observed, probably associated with insufficient river load (Richon et al.,
353 2019; Reale et al., 2020a) and with the tendency of satellite chl-*a* measures to be systematically overestimated in the
354 coastal areas with respect to "in situ" observations due to the presence of particulate suspended matter in the water column
355 (Claustre et al., 2002; Morel et Gentili, 2009).

356 Figure 2 also shows the average vertical profiles, computed for the entire, Western and Eastern Mediterranean basins, of
357 chl-*a* (c), PO_4 (d), NO_3 (e), dissolved oxygen (f), DIC (g), pH (h) and ALK (i) in the CTRL compared with the recent
358 CMEMS reanalysis (only for chl-*a* and pH, Cossarini et al., 2021) and EMODnet datasets (European Marine Observation
359 and Data Network; Buga et al., 2018). In spite of the tendency to overestimate the chl-*a* values, the model captures the
360 DCM location, the west-east trophic gradient in the basin, and also the nutricline depths deepening between Western and
361 Eastern basin and the low nutrient surface concentrations. Mean simulated values in the first 0-200 m are quite realistic
362 for almost all the biogeochemical tracers and properties, with correlation values between observations and modelled data
363 greater than 0.93. At the same time, the CTRL overestimates the PO_4 concentration between 100 and 300 m of about 50%,
364 and the dissolved oxygen concentration of about 15% below 200 m and underestimates, below 200 m, the NO_3
365 concentration of about 20% and the pH of about 1 % between 100 and 300 m. It is worthwhile to point out that the limited
366 spatial resolution of the observations below 200 m could impact the robustness of our comparison. In general, the biases
367 in the initial conditions are originated by the spin-up simulation that allows to remove the largest part of model drifts. As
368 explained in section 2.4, these biases, which are still present in both the CTRL and scenario simulations, do not affect the
369 calculation of the climate change signals, and are generally lower than the changes observed in the scenarios at the end
370 of the century.

371 To summarize, although the model shows some deficiencies in simulating the vertical distribution of some
372 biogeochemical tracers and properties, the main features of the system are reliably simulated and thus, MFS16-OGSTM-
373 BFM is robust enough to be used to investigate the evolution of the Mediterranean biogeochemistry under different
374 emission scenarios.

375
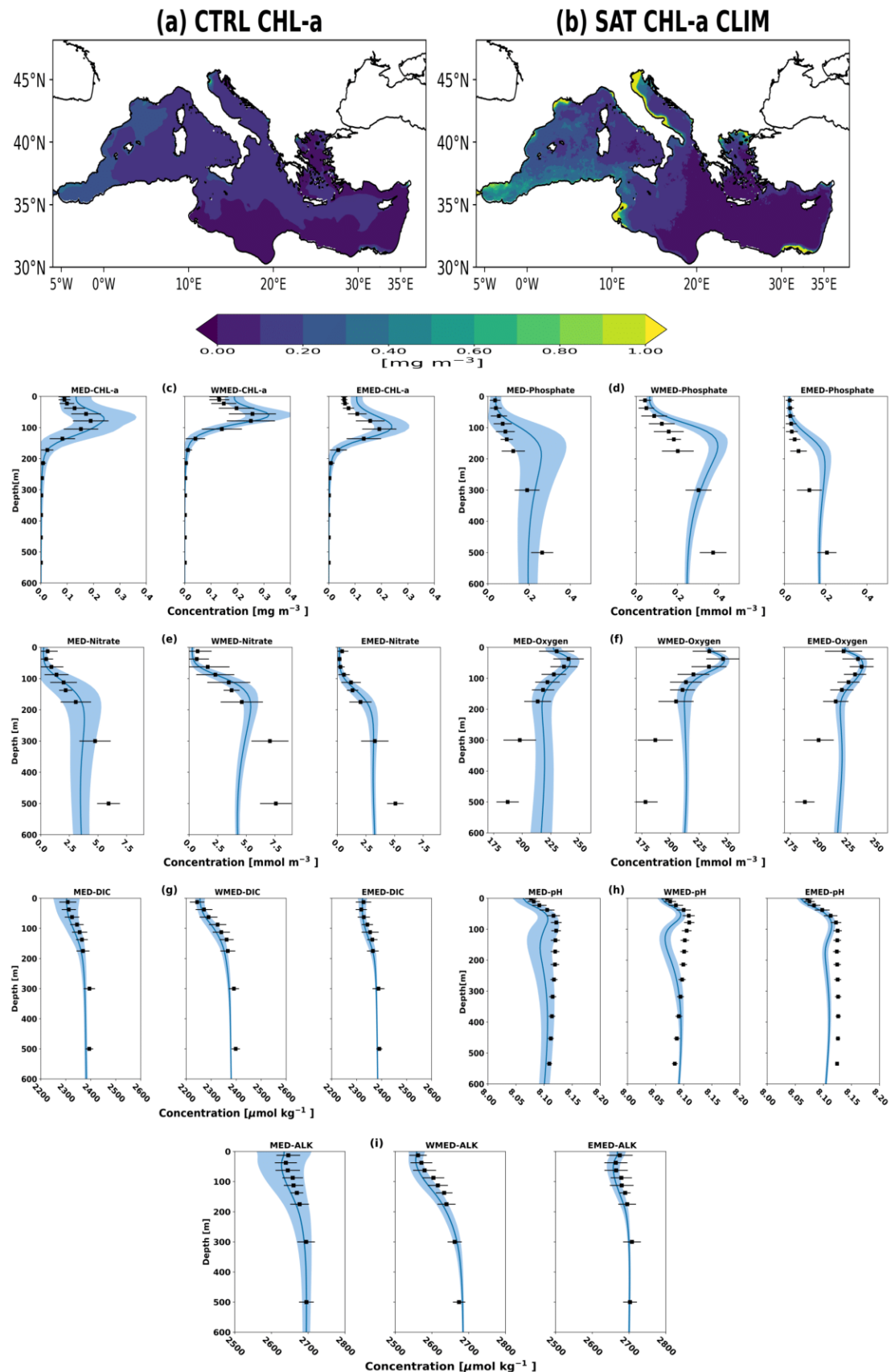
376
377
378 **Fig.2 Average chl-*a* in the first 10 m in CTRL (a) for the period 2005-2020 and CMEMS-SAT (b) together with CTRL average**

379 **vertical profiles (blue lines) for the period 2005-2020 of chl-*a* (c, mg m⁻³), PO₄ (d, mmol m⁻³), NO₃ (e, mmol m⁻³), Dissolved**

oxygen (f, mmol m^{-3}), DIC (g, μmol kg^{-1}), pH (h) and ALK (i, μmol kg^{-1}). The averaged profiles are computed for the entire (MED), Western (WMED) and Eastern (EMED) Mediterranean Sea. The light blue areas represent the spatial standard deviation of the monthly model data. The model data are compared with CMEMS reanalysis (chl-*a* and pH; Colella et al., 2016: Teruzzi et al., 2021) and observations provided by EMODnet (PO$_4$, NO$_3$, Dissolved oxygen, DIC, ALK; Buga et al., 2018): annual mean (black squares) and related standard deviations (black bars). Depth is measured in meters.

3.2 Evolution of the thermohaline properties and circulation of the Mediterranean Sea in the 21st century

Mean temperature and salinity evolution between 0-100 m and 200-600 m in the 2005-2099 period under the RCP4.5 and RCP8.5 scenarios in the whole Mediterranean Sea and in the Western and Eastern basins are shown in Fig. 3. As for the biogeochemical variables, these depths have been chosen as they are representative of the location of MAW and LIW, respectively.

A warming of the surface and intermediate layers is observed at the basin scale and in both the Western and Eastern basins, whose magnitude (approximately 1.5 °C in the RCP4.5 and 3°C in the RCP8.5 scenario) agrees with what has already been observed in recent modelling studies based on single/multimodel ensembles (e.g., Adloff et al., 2015; Soto-Navarro et al., 2020).

Similar to the seawater temperature, the variation in salinity is strongly dependent on the emission scenario with more intense anomalies, both negative and positive, under RCP8.5 conditions (as observed in previous modelling studies such as Adloff et al., 2015 and Soto-Navarro et al., 2020). For example, salinity in the surface layer at basin scale and in the Eastern basin is characterized by a decrease between 2020 and 2050 followed by a constant increase (stronger under RCP8.5 scenario) until the end of the 21st century. Conversely, after 2050, the Western basin shows a freshening of the surface layer with respect to the beginning of the century, in agreement with what was already observed by Soto-Navarro et al. (2020). An increase in salinity also occurs in both scenarios in the intermediate layer both at the basin scale and in the two main sub-basins.
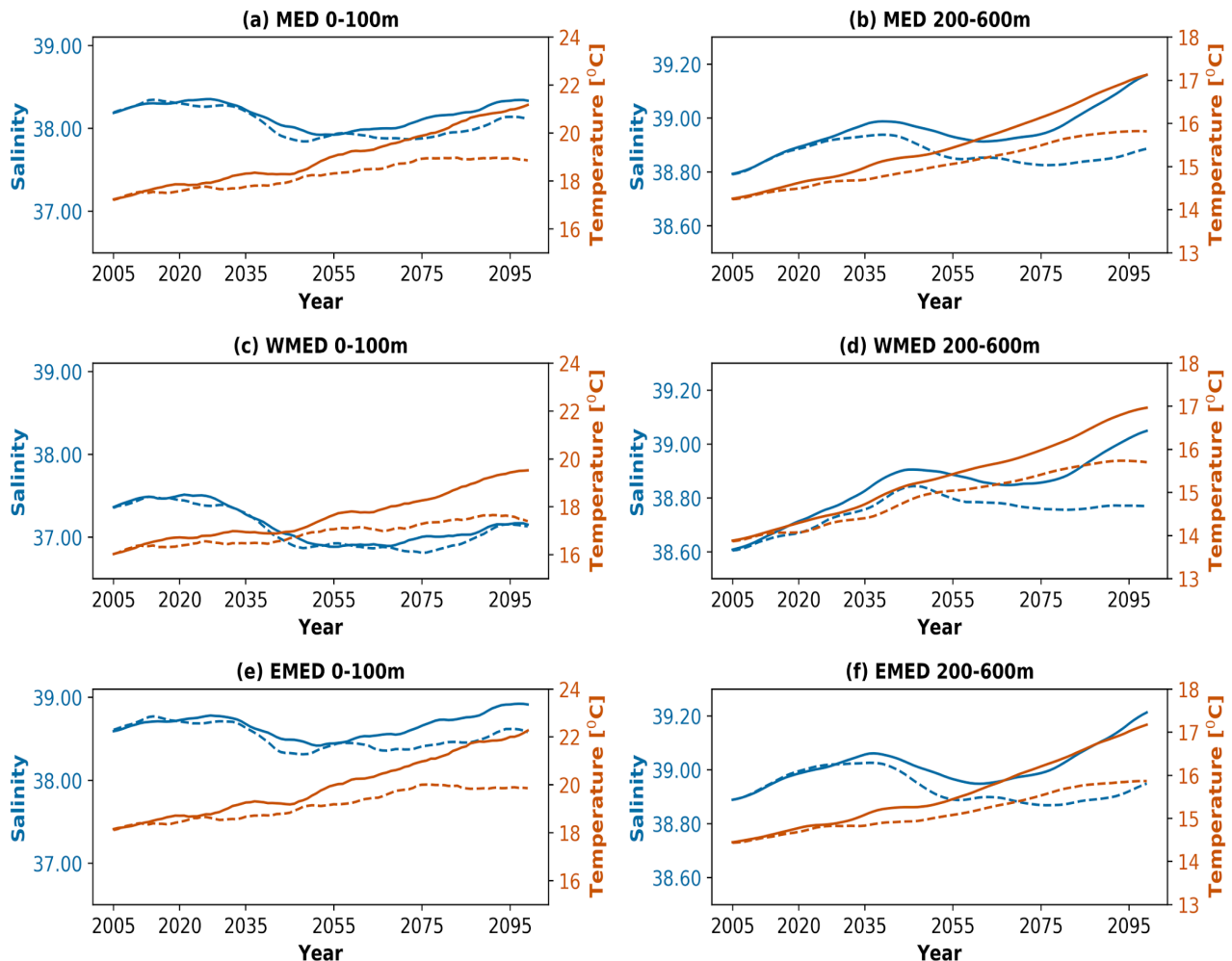
Fig.3 - Yearly time series for the period 2005-2099 of Salinity (blue) and Temperature (dark orange, in ºC) under the emission scenarios RCP8.5 (solid line) and RCP4.5 (dashed line) in the Mediterranean Sea (MED, a-b), Western Mediterranean (WMED, c-d) and Eastern Mediterranean (EMED, e-f) for the layers 0-100 m (left column) and 200-600 m (right column). The yearly time series have been smoothed using 10-years running mean.

The spatial distribution of temperature variations in the surface layer (Fig. S2) shows a comparable and mostly statistically significant on basin-scale warming in RCP4.5 and RCP8.5 in the MID-FUTURE (the differences between the projected changes are lower than 2%), while, in the FAR-FUTURE, the projected changes in the RCP4.5 are approximately the 50% lower with respect those observed in RCP8.5 (8-12% and 17-20% respectively), with the North Western Mediterranean, Tyrrhenian, Adriatic, Ionian, Aegean Sea and Levantine, being the most affected sub-basins. Local relative maxima are observed in both scenarios, in the Gulf of Lion, in the relatively shallow and in the coastal areas of the Adriatic Sea and in the area of the Rhodes Gyre (Fig.S2 i,j).

A general freshening of the upper layers and saltening of the intermediate layers over most of the Mediterranean basin is observed during the MID-FUTURE period (Fig. S3). The projected changes are statistically significant over most of the basin with the only exception, in both scenarios, of the upper layer of the Adriatic Sea and Northern Ionian Sea and the intermediate layers of the Southern Ionian and Levantine Basin/Southern Adriatic and Northern Ionian Sea in the RCP4.5/RCP8.5 scenario as consequence, probably, of the river input in the Adriatic Sea and mid-Ionian Jet dynamics.

The latter has been recognized, in fact, as an important driver for the salinity for the upper and intermediate layers of the Adriatic and Ionian Sea (e.g. Gacic et al., 2010). In the FAR-FUTURE, the freshening of the surface is still present at the basin scale in the RCP4.5 scenario (although it is reduced with respect to the MID-FUTURE) and in the Western basin in the RCP8.5 scenario. Moreover, an increase in salinity is observed in the Adriatic Sea and in the Eastern basin under RCP8.5. The projected changes in the surface salinity in the Adriatic Sea and Northern Ionian Sea under RCP4.5 are also not significant.

The decrease in salinity in the 21st century in the Western basin is driven by the salinity values imposed in the Atlantic buffer zone (Lovato et al., 2013), while the saltening of the Eastern basin, under RCP8.5 scenario, is linked to the decreasing freshwater discharge in the area (e.g., Gualdi et al., 2013; Soto-Navarro et al., 2020). In the intermediate layer, the situation is reversed: while in RCP8.5 the entire basin experiences an increase in the salinity associated with the increase in salinity in the surface water of the Eastern basin, in RCP4.5 the Eastern basin experiences a slight decrease in salinity associated again with the freshening of surface water. In fact, at the surface, both signals are transported by vertical mixing to the intermediate layers of the Eastern basin influencing the salinity of the newly formed LIW.

Figure 4 shows the temporal evolution of the Mediterranean thermohaline circulation during the 21st century using the zonal overturning stream function (or ZOF; Myers and Haines, 2002; Somot et al., 2006). The ZOF has been computed by the meridional integration from south to north and from the bottom to the top of the water column of the zonal velocity (see Adloff et al., 2015). The domain of the integration is the same as shown in Figure 1 with the exclusion of the Atlantic area outside the Strait of Gibraltar. The thermohaline circulation of the basin in the PRESENT is composed of two cells, similar to the outcomes of the historical reference experiments described in Adloff et al. (2015) and Waldman et al. (2018). The first cell extends from the surface to 800 m, with a clockwise circulation associated with MAW moving eastwards and LIW moving westwards. The second cell is located between 500 and 2500 m in the Eastern Mediterranean with a counterclockwise circulation associated with the Eastern Mediterranean Deep Water (EMDW) moving eastwards and LIW moving westwards.

Under the two scenarios, during the MID-FUTURE period, there is an evident weakening of both cells and a reduction of the thickness of the upper layer cell and the Eastern basin cell (less than -0.1 Sv), which splits into two sub-cells. By the end of the century both cells show a similar behavior, whereas in the RCP4.5 scenario, the Eastern cell is slightly more intense. The weakening of the zonal overturning stream function is similar to previous findings of Somot et al. (2006) and Adloff et al. (2015). As the Mediterranean thermohaline circulation is driven by both deep and intermediate water formation processes, the overall weakening of both cells is a direct consequence of the increase in the vertical stratification of the water column. In fact, the evolution of the winter maximum mixed layer depth in key convective areas of the Mediterranean Sea, such as the Gulf of Lion, Southern Adriatic, Aegean Sea and Levantine basin (Fig. S4), shows a progressive decrease in the intensity of the open ocean convection after 2030. Only for the Aegean Sea, the changes in the winter mixed layer maximum depth are less marked, with the occurrence of some maxima around 2080 (in RCP8.5) or after 2090 (in RCP4.5), which could correspond to a future tendency of the thermohaline circulation of the Eastern basin to produce EMT (Eastern Mediterranean Transient)-like events (Adloff et al., 2015).

467 The projected overall weakening of the Mediterranean thermohaline circulation leads to a reduction in the exchanges of

468 biogeochemical properties between the Western and Eastern basins through the Strait of Sicily at both the surface and

469 intermediate levels (Fig. S5) and to a reduced ventilation of intermediate/deep waters (Adloff et al., 2015).

470

471
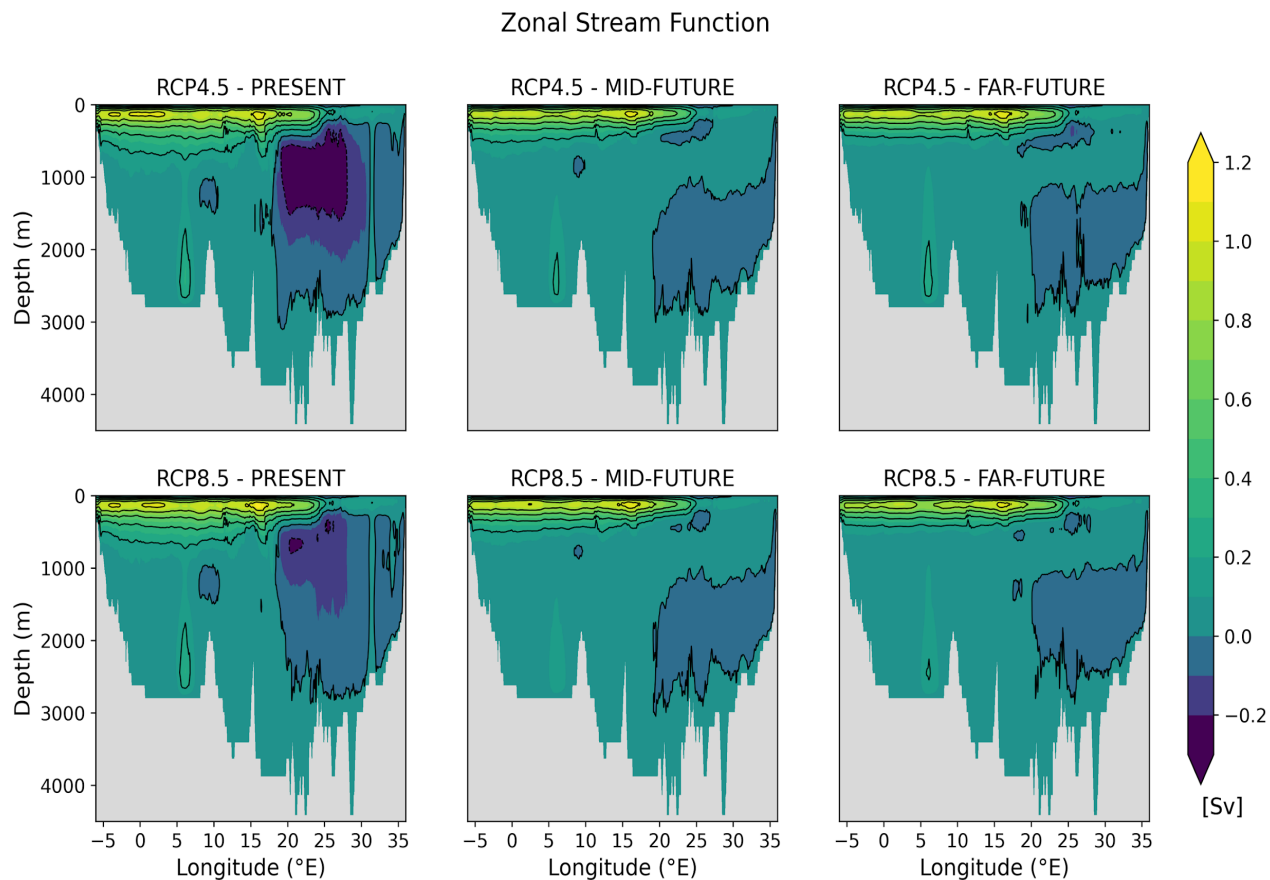
472

473 **Fig. 4 - Mediterranean Sea zonal stream function annual mean (in Sv) averaged over the PRESENT (2005-2020), MID-**

474 **FUTURE (2040-2059) and FAR-FUTURE (2080-2099) periods under RCP4.5 and RCP8.5 scenarios.**

475

476 **3.3 Spatial and temporal evolution of nutrients, dissolved oxygen and chl-*a* concentrations**

477

478 Figures 5 and 6 show the spatial distribution of the magnitude and signs of the changes that will affect the dissolved

479 nutrient concentrations during the 21st century. In the FAR-FUTURE, the decreases in PO_4 and NO_3 concentrations in

480 the 0-100 m layer are almost half in RCP4.5 (approximately 7% and 13% for PO_4 and NO_3, respectively) with respect to

481 those observed in the RCP8.5 (approximately 13% and 20% for PO_4 and NO_3, respectively) and are particularly marked

482 and statistically significant in the Levantine basin, in the Aegean Sea, in the Central/Southern Adriatic Sea and Northern

483 Ionian Sea. Again, statistically significant relative local maxima (in absolute value) are observed in both scenarios in the

484 area of the Gulf of Lion, Southern Adriatic, Northern Ionian and Rhodes Gyre. Moreover, there are clear spatial gradients

485 affecting the statistical significance of the projected changes. For example, the projected changes in nutrient concentration

486   in the Northern Adriatic Sea and in many other coastal areas, influenced by river dynamics, are not significant, contrary

487   to what is observed in the open ocean areas of the same sub-basin. Here, the projected decrease is associated with the

488   reduced vertical mixing in the water column and reduced inflow of nutrients through the Otranto Strait (Fig. S6). Finally,

489   the two scenarios show some significant changes in the dissolved nutrient concentrations at local scale in the Alboran Sea

490   and in the Southern Ionian associated with changes in the intensity of mesoscale circulation (eddies) of both areas and in

491   the intensity and spatial structure of the mid-Ionian jet (not shown).

492

493   In contrast to the general decreasing nutrient content of the upper layer, the intermediate layer in both scenarios shows a

494   strong (milder) increase in nutrient concentration in the Southern Aegean Sea (Levantine basin, North Western

495   Mediterranean and Alboran Sea) in the 21st century driven by the reduced vertical mixing, which tends to increase the

496   nutrient content of the intermediate layers. The Tyrrhenian, Ionian and Southern Adriatic Seas are, in turn, characterized

497   by a permanent negative anomaly. In the first two areas, the anomaly can be associated with the decrease in the westward

498   transport of nutrients in the intermediate layers through the Strait of Sicily (consequences of the weakening of the zonal

499   stream function discussed in Section 3.2, Fig. S5), while in the Adriatic Sea, the projected changes are driven by the

500   increase in the nutrient export in the intermediate layer through the Otranto Strait (Fig. S6). In the North Western

501   Mediterranean, the observed positive anomalies become weaker and even negative in the FAR-FUTURE under the

502   RCP4.5 emission scenario, likely due to some convective events that take place between 2080 and 2100, as shown in Fig.

503   S4. Comparing the projected changes at the surface in the FAR-FUTURE it is observed that while under RCP4.5 in most

504   of the Western Mediterranean and the Ionian Sea they are not statistically significant, under RCP8.5 emission scenario

505   the statistical significance that was initially limited to Adriatic, Aegean Sea and Levantine basin, now it also involves the

506   Ionian and Tyrrhenian Sea.

507

PO$_4$
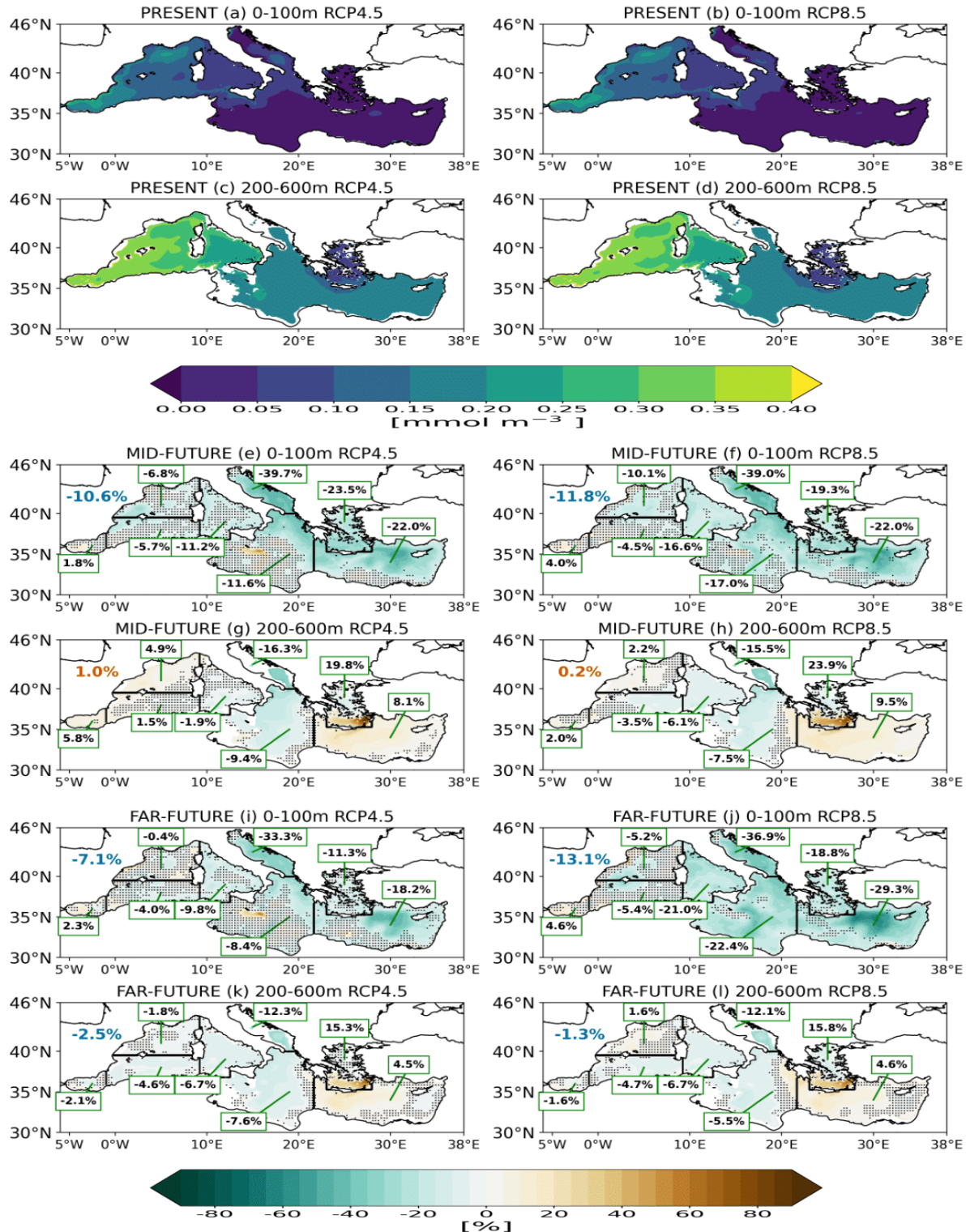
508

509 **Fig. 5 - Phosphate concentration (in mmol m^{-3}) in the layers 0-100 m and 200-600 m in the PRESENT (2005-2020, a,b,c and d),**

510 **and relative climate change signal (with respect to the PRESENT) in the MID-FUTURE (2040-2059, e,f,g and h) and FAR-**

511 **FUTURE (2080-2099, i,j,k and l) in the RCP4.5 (left column) and RCP8.5 (right column) emission scenario. The Mediterranean**

512 **average relative climate change signal in each period (with respect to the PRESENT) is displayed by the top-left colored value**

513 **(blue or dark orange when negative or positive). Values in the green boxes are the average relative climate change signal in**

514   **each period and in each sub-basin shown in Figure 1. Domain grid points where the relative climate change signals are not**

515   **statistically significant according to a Mann-Whitney test with p<0.05 are marked by a dot.**

516
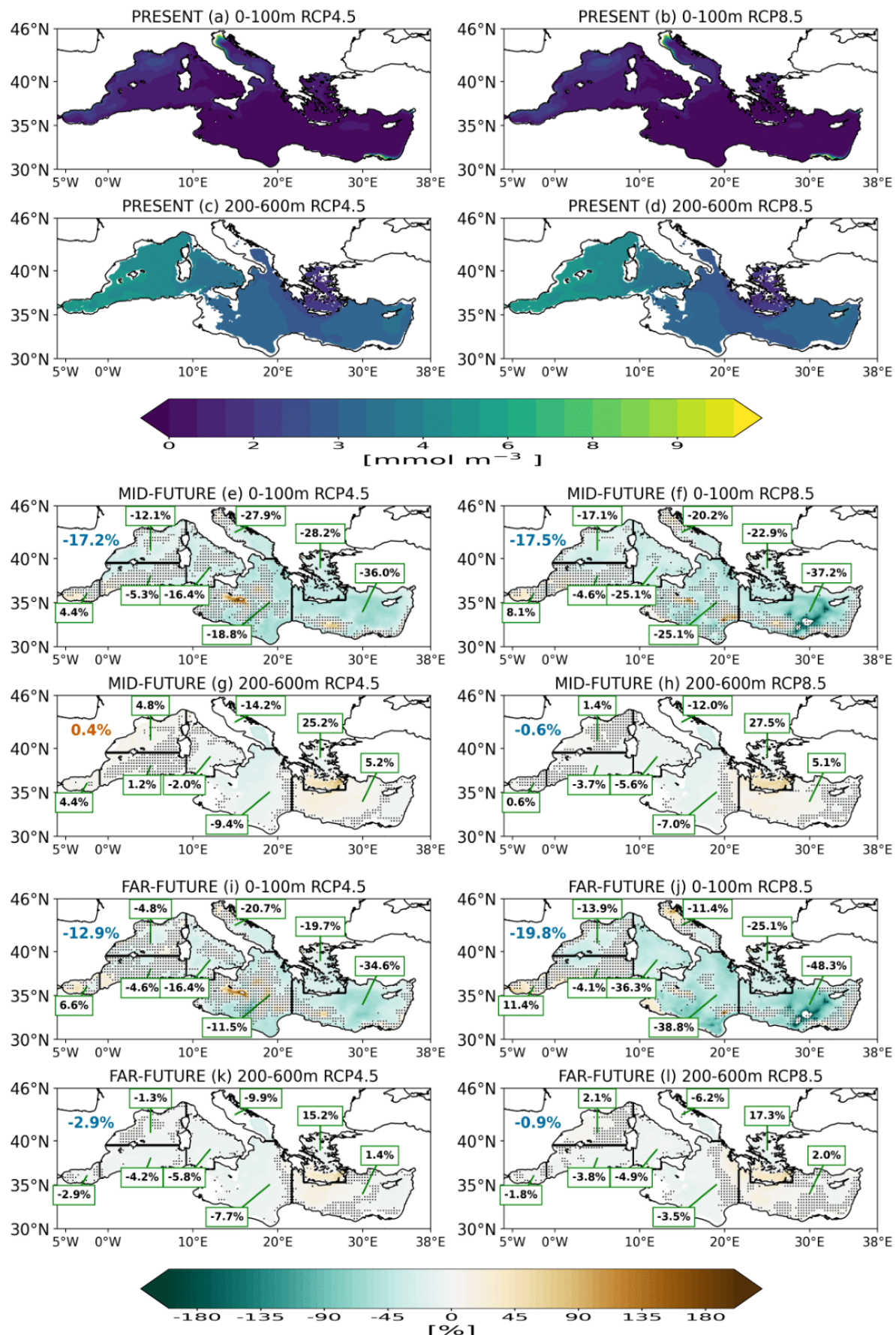
Fig.6 - as Fig.5 but for Nitrate (in mmol m^{-3})

The temporal evolution of the mean concentrations of PO_4 and NO_3 in the RCP4.5 and RCP8.5 simulations between 0-100 m and 200-600 m in the Mediterranean Sea and its Western and Eastern basins for the 2005-2099 period is shown in Fig. 7. In the RCP8.5 scenario, PO_4 and NO_3 concentrations within the euphotic layer of both sub-basins are substantially stable for the first 30 simulated years, while a marked decline occurs after 2030-2035, with values of 0.01 and 0.1 mmol m^{-3} (compared to the beginning of the century) respectively, which is followed by a steady evolution of the concentration values until the end of the century. The same behaviour is observed in RCP4.5, except for a recovery that takes place at the end of the century in correspondence to an increase in the nutrient inflow into the Alboran Sea (Fig. S7). The observed decline is timely in phase with the weakening of the zonal stream function discussed in Fig. 4, further pointing out the importance of the vertical mixing in driving the temporal variability of nutrients in the euphotic layer. From this point of view, some relative maxima of both nutrient concentrations in the Western and Eastern basins are observed for RCP4.5 in the 2015-2040 period (Fig. 5 c,d), associated with strong ocean convective events taking place in the Gulf of Lion and Levantine basin (Fig. S4). Between 2055 and 2075, the peak in both nutrients' concentration, for RCP4.5, timely corresponds to a peak in the inflow of nutrients into the Alboran Sea (Fig. S7). Additionally, in both the scenarios, the intermediate layer of the Western basin, after 2035, experiences a negative tendency in the nutrient concentration (greater than 0.01 mmol m^{-3} for PO_4 and 0.1 mmol m^{-3} for NO_3) related to a reduced westward transport of nutrients associated with LIW (Fig.S5).
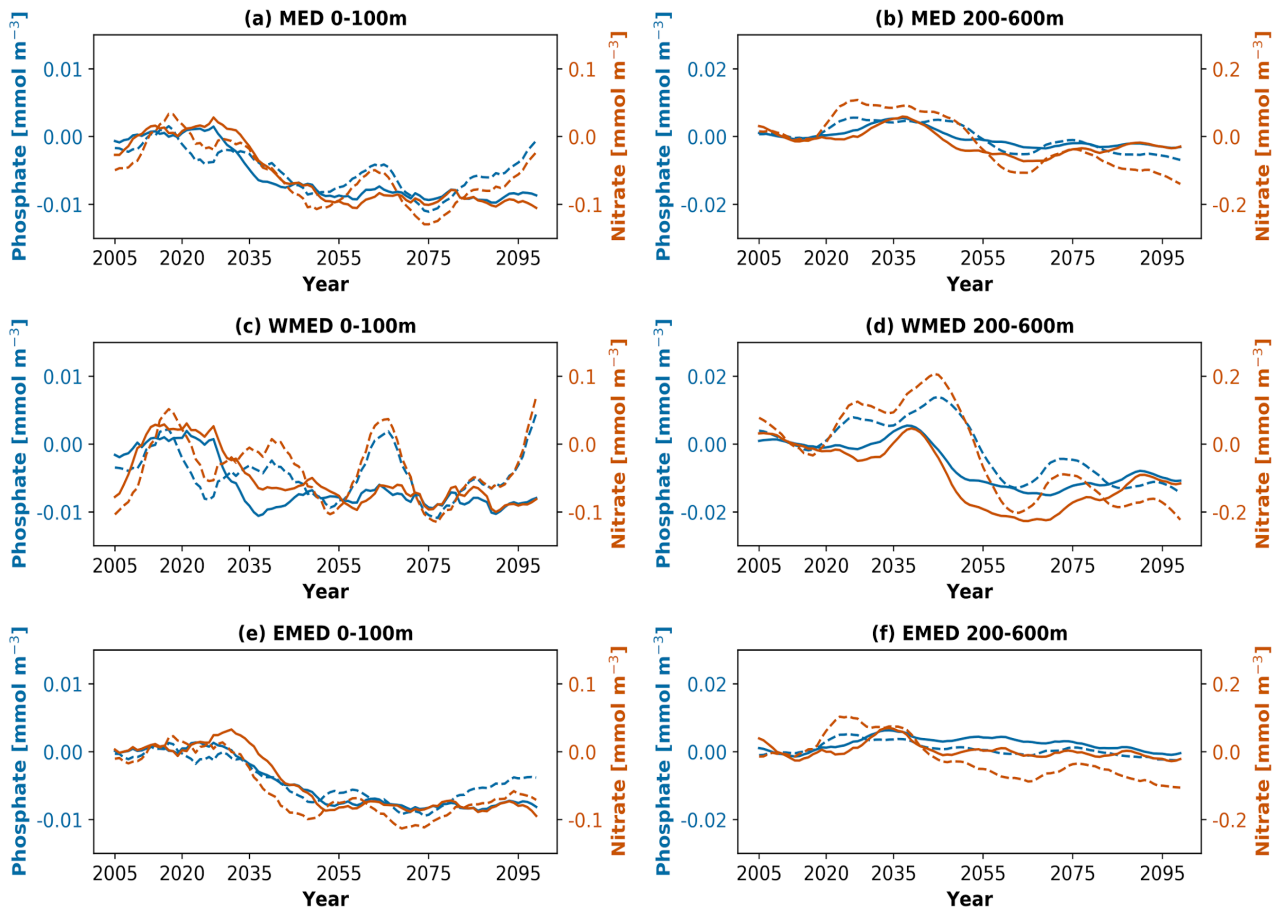
539

540 **Fig.7 - Yearly time series for the period 2005-2099 of Phosphate (blue, in mmol m^{-3}) and Nitrate (dark orange, in mmol m^{-3})**
541 **anomalies for the emission scenario RCP8.5 (solid line) and RCP4.5 (dashed line) in the Mediterranean Sea (MED, a-b),**
542 **Western Mediterranean (WMED, c-d) and Eastern Mediterranean (EMED, e-f) for the layer 0-100 m (left column) and 200-**
543 **600 m (right column). The yearly time series have been smoothed using 10-years running mean.**

544

545 The temporal evolution of chl-*a* in the two scenarios is similar to what was observed in the case of dissolved nutrients,

546 with a high interannual variability, a decrease after 2030-2035 of approximately 0.03 mg m^{-3} and a stable signal until the

547 end of the century in the RCP8.5 scenario while, in the case of the RCP4.5 a recovery towards the observed PRESENT

548 values is simulated at the end of 21st century (Fig.8). In the Eastern Mediterranean the decrease is of the same magnitude

549 as that observed at the basin scale, while in the Western basin the chl-*a* signal appears substantially stable with respect to

550 the present.

551
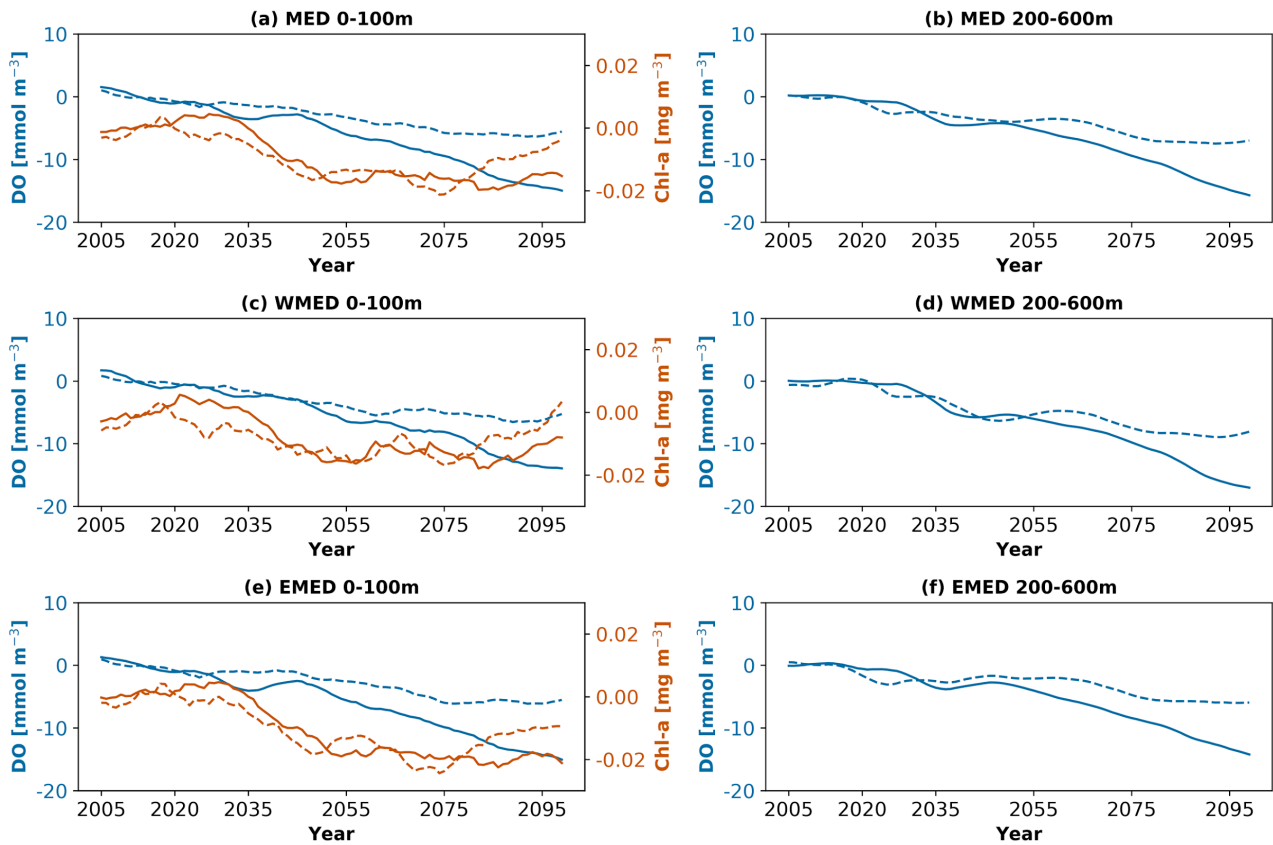
Fig. 8 as Fig.5 but for Dissolved Oxygen (blue, in mmol m⁻³) and Chl-*a* (dark orange, in mg m⁻³)

During the 21st century, a continuous decrease in the oxygen concentration is projected in both scenarios in the Mediterranean Sea (Fig. 8). The simulated reduction of the oxygen values is slower in the RCP4.5 with respect to RCP8.5. For example, under the RCP8.5 emission scenario, the concentration of the dissolved oxygen in the upper layer decreases by approximately 15 mmol m⁻³, which is three times the value observed in the RCP4.5 scenario (Fig. 8). The decrease in dissolved oxygen is rather uniform and almost statistically significant everywhere in both the horizontal and vertical directions in all the sub-basins, with values that are half in RCP4.5 (in percentages) with respect to those observed under RCP8.5 (Fig. S8). For example, the decrease in the oxygen concentrations in the Levantine basin, in the FAR-FUTURE, is approximately equal to 3% under the RCP4.5 emission scenario and 6% under the RCP8.5 emission scenario. In the North Western Mediterranean, these values are approximately 3% and 7% respectively. The projected decreases in both scenarios are usually lower in the Alboran Sea and South Western Mediterranean with respect to the rest of the basin, as a consequence of the damping effect driven by the oxygen values imposed at the Atlantic boundary. In fact, the advection of dissolved oxygen associated with AW partially limits the reduction in the oxygen solubility at the surface as a consequence of the warming of the water column in the sub-basins near the Strait of Gibraltar, such as the Alboran Sea.

The uniform decrease in the oxygen surface concentration observed in Fig. S8 is spatially coherent (also from the statistical point of view) with the increase in the temperature shown in Fig. S4, confirming the importance of temperature in driving the solubility of the oxygen in the marine environment (Keeling et al., 2010; Shepherd et al., 2017). Moreover, a decrease in the oxygen inflow (not shown) into the Alboran Sea and an overall increase in community respiration (see the analysis related to the phytoplankton respiration in section 3.4) are found, which represent additional factors explaining the projected changes. Western sub-basins, deep convection areas and shallow coastal zones of the Adriatic

575 Sea are the regions that show the highest decrease of oxygen in both surface and intermediate layer, with again the

576 magnitude of the observed signal depending on the considered scenario (Fig. S8) and related to the reduction in vertical

577 processes's intensity. The effect of the increased stratification on the oxygen vertical distribution is clearly shown in

578 Figure 9. Under RCP8.5 (Fig.9 a,b), the progressive decline of oxygen concentration is timely corresponding to the

579 progressive decrease in the maximum mixed layer depth (Fig. S4) and the weakening of the zonal stream function (Fig.4)

580 discussed in Section 3.2. For example, in the North Western Mediterranean the correlation coefficient between the average

581 dissolved oxygen concentration in the first 100 m and the maximum mixed layer depth has been found equal to 0.64

582 (statistically significant with $p < 0.05$). On the other hand, under the RCP4.5 emission scenario, some events of deep

583 transport of oxygen, that dumped the decline in the oxygen concentration, can be recognized towards the end of the 21st

584 century in both Western and Eastern Mediterranean.

585

586
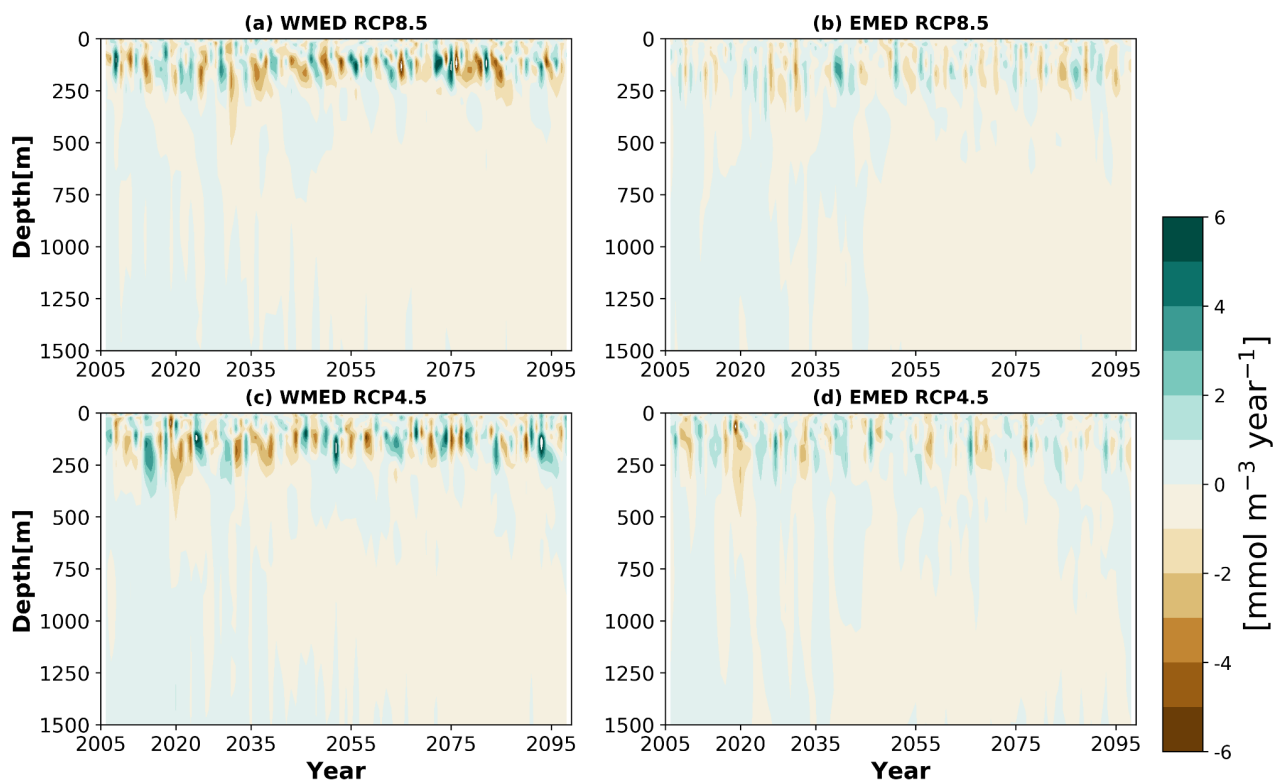
587

588 **Fig.9 Annual rate of change of Dissolved Oxygen (mmol m⁻³ year⁻¹) in the Western (a,c) and Eastern (b,d) Mediterranean Sea**

589 **in RCP8.5 (a,b) and RCP4.5 (c,d).**

590

591 **3.4 Spatial and temporal evolution of net primary production and living/non-living organic matter**

592

593 The warming of the water column and the increase in vertical stratification affect the metabolic rate of ecosystem

594 processes including CO_2 fixation and community respiration. In fact, a basin-wide increase in net primary production

595 (NPP) starting after 2035 and proceeding until the end of the simulations, is projected in both scenarios (Fig. 10). In the

596 RCP4.5 scenario the NPP increase is greater than 10 gC m⁻² year⁻¹, which is a value that is more than half with respect to

597 the values observed in the RCP8.5 simulation.

598

599
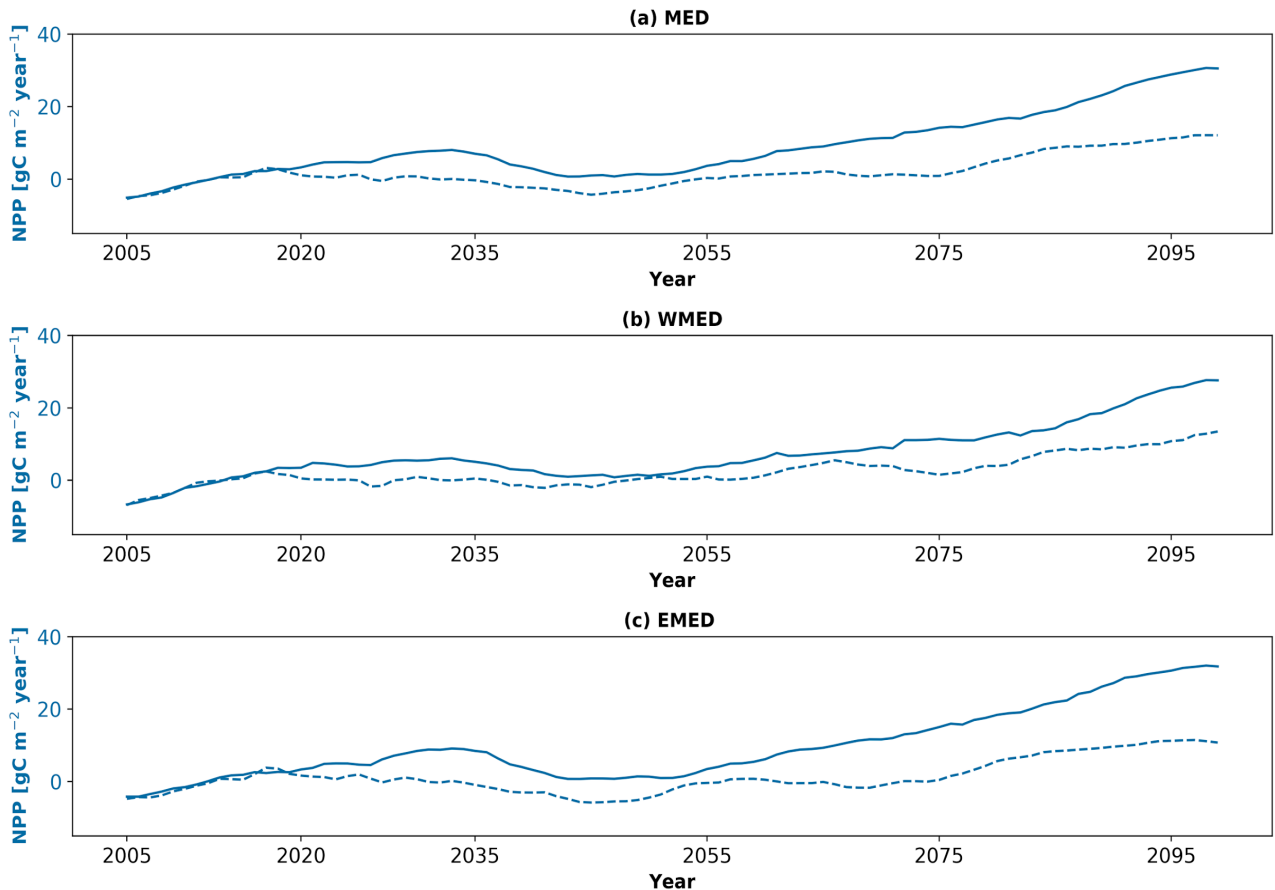
Fig.10 - Yearly time series for the period 2005-2099 of Integrated net primary production (blue, in gC m^{-2} year^{-1}) anomalies for the emission scenario RCP8.5 (solid line) and RCP4.5 (dashed line) in the Mediterranean Sea (MED, a), Western Mediterranean (WMED, b) and Eastern Mediterranean (c) for the first 200 m. The yearly time series have been smoothed using 10-years running mean.

The distribution of the sign of the NPP changes is not uniform across the basin and between the simulations (Fig.11). In the MID-FUTURE, in both scenarios, the only areas that experience an increase (not statistically significant in all the cases) in the NPP with respect to the beginning of the century are the North Western Mediterranean, the Tyrrhenian Sea, the Northern Adriatic Sea, part of the Ionian Sea and of the Levantine basin. Conversely, the only statistically significant projected changes are negative and are observed in the Central and Southern Adriatic Sea, part of the Northern Ionian Sea and the Rhodes Gyre areas. The Aegean Sea shows a rather opposite behavior with a negative/positive anomaly in RCP4.5/RCP8.5. In the FAR-FUTURE, corresponding to a more pronounced warming of the basin, the NPP increase is quite uniform and statistically significant over most of the basin and is equal approximately equal to 7% in RCP4.5, which is approximately the half of value observed in the RCP8.5 (approximately 17%). Under the RCP8.5 emission scenario there is a 7-to-23% increase in NPP throughout the basin, with the relative local maxima observed mainly in the coastal areas of the North Western Mediterranean, Levantine basin, Northern Adriatic Sea, Gulf of Lion, Aegean Sea (similar results, although with lower rates, were found at the end of the 21st century by Solidoro et al., 2022). Conversely, under the RCP4.5 scenario, the Adriatic Sea is still characterized by a negative and not significant anomaly (-1%), while for the rest of the basin the sign of the anomaly is positive and statistically significant, with the greatest values observed in the North Western Mediterranean (approximately 12%, which is almost half of the variation observed in the RCP8.5 scenario). In both scenarios, a negative anomaly is observed in the Rhodes gyre area, which is extremely weak in RCP8.5.

621 Both negative anomalies are temporally consistent with some convective events taking place in both areas after 2080 and
622 shown in Fig. S4.
623
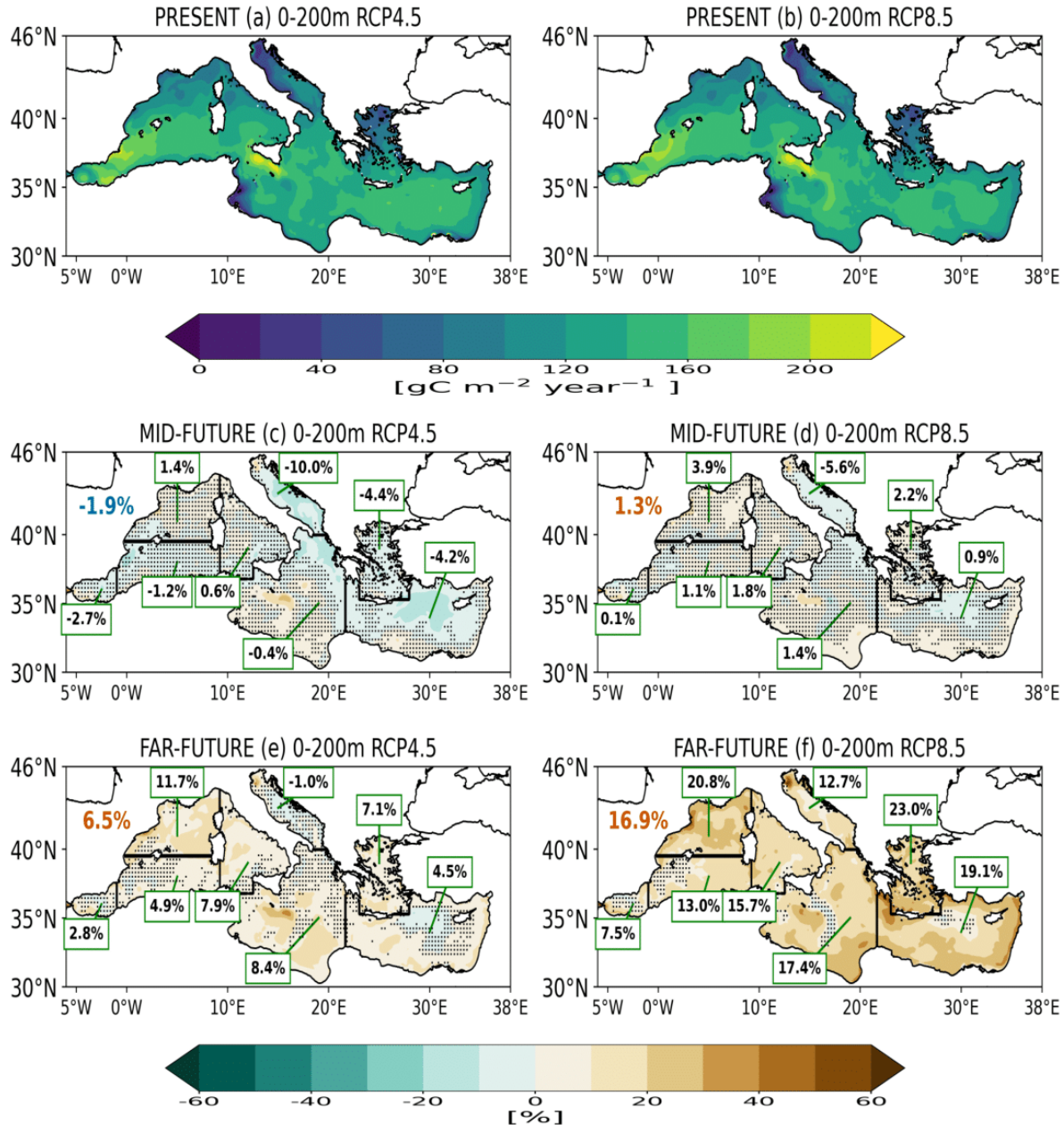
624
625 **Fig. 11 - Integrated net primary production variation (in gC m⁻² year⁻¹) in first 0-200 m in the PRESENT (2005-2020, a,b),**
626 **and relative climate change signal (with respect to the PRESENT, in units of pH) in the MID-FUTURE (2040-**
627 **2059, c,d) and FAR-FUTURE (2080-2099, e,f) in the RCP4.5 (left column) and RCP8.5 (right column) scenarios.**
628 **The Mediterranean average relative climate change signal in each period (with respect to the PRESENT) is**
629 **displayed by the top-left colored value (blue or dark orange when negative or positive). Values in the green boxes**
630 **is the average relative climate change signal in each period and in each sub-basin shown in Figure 1. Domain grid**

As shown by Lazzari et al. (2014) and Solidoro et al. (2022), the overall warming of the water column also results in an increase in community respiration. In agreement with that, Fig. S9 shows the spatial distribution of phytoplankton respiration (RESP) changes in the MID-FUTURE. It is possible to observe some differences with respect to NPP. In both scenarios, there is an overall decrease in the RESP with respect to the beginning of the 21st century, which is approximately equal to -4% in the RCP4.5 and -2% in the RCP8.5. In both scenarios the projected changes are again positive and not statistically significant in the Northern Adriatic, most of the North Western Mediterranean, Central and Southern Ionian and coastal areas of the Levantine basin. As previously observed for NPP, the Adriatic Sea has an overall negative and statistically significant anomaly, as well as the Northern Ionian Sea and the area of the Rhodes gyre. The North Western Mediterranean is the only area where the variation has an opposite sign in two scenarios: it is negative (-1.4%) in RCP4.5 and positive (approximately 1%) in RCP8.5.

In the FAR-FUTURE, the pattern of variation is coherent with that already observed in the NPP (Fig. 11). RESP increases at the end of the 21st century over the entire basin of approximately 5% (11%) in RCP4.5 (RCP8.5). Under the RCP4.5 scenario, the Adriatic Sea, with the northern part as the only exception, and the Rhodes gyre area are still characterized by a negative anomaly while under RCP8.5, the highest values are observed in the North Western Mediterranean (this is also true for the RCP4.5 scenario), Aegean Sea and Levantine basin.

The overall increase in the respiration community has as a consequence the decrease in the organic stock matter in the water column. The temporal evolution of the carbon organic matter standing stock for the 2005-2099 in RCP4.5 and RCP8.5 simulations between 0-100 m and 200-600 m in the whole Mediterranean and in its Western and Eastern basins is shown in Figure 12. The evolution of the carbon organic matter standing stock is similar to that observed in the dissolved nutrients, with a substantially stable signal in the first 30 years of the 21st century and a decrease after 2030. Afterwards, while RCP4.5 shows a recovery at the end of the 21st century, the projected decline in the RCP8.5 is approximately equal to 5 mgC m^{-3}. The same dynamics is observed in the intermediate layer, where the decline after the period 2030-2035 is approximately equal to 0.3 mgC m^{-3} for the carbon stock.

Similar dynamics are also observed for plankton (both phyto and zoo, Fig. 13), bacterial biomass and particulate organic matter in the euphotic layer (Fig. 14). In the RCP4.5 simulation for all these biogeochemical tracers, a recovery in the biomass at the end of the 21st century is found and the projected changes are approximately 50% with respect to the RCP8.5 scenario where no recovery is observed. In particular, the decrease of the phytoplankton (zooplankton) biomass is approximately 2 (1.5) mgC m^{-3} and appears to be stronger in the Eastern than in Western basin. Under RCP8.5 the bacterial biomass is projected to decrease at the basin scale by the end of the century by approximately 0.5 mgC m^{-3}, by 0.2 mgC m^{-3} in the Western basin and by 0.6 mgC m^{-3} in the Eastern basin. Finally, the decline in particulate organic matter is approximately 1.5 mgC m^{-3} at the basin scale, approximately 1 (2) mgC m^{-3} in the Western (Eastern) basin. In the intermediate layer, the decline of the bacterial biomass in the entire basin is fairly uniform and continuous until the end of the 21st century, with a variation of approximately 0.3 mgC m^{-3} with respect to the beginning of the century. For

671 the same layer, particulate organic matter declines after the period 2030-2035 but successively the signal remains

672 substantially stable and, in particular in the Western basin, tends to recover at the end of the century.

673
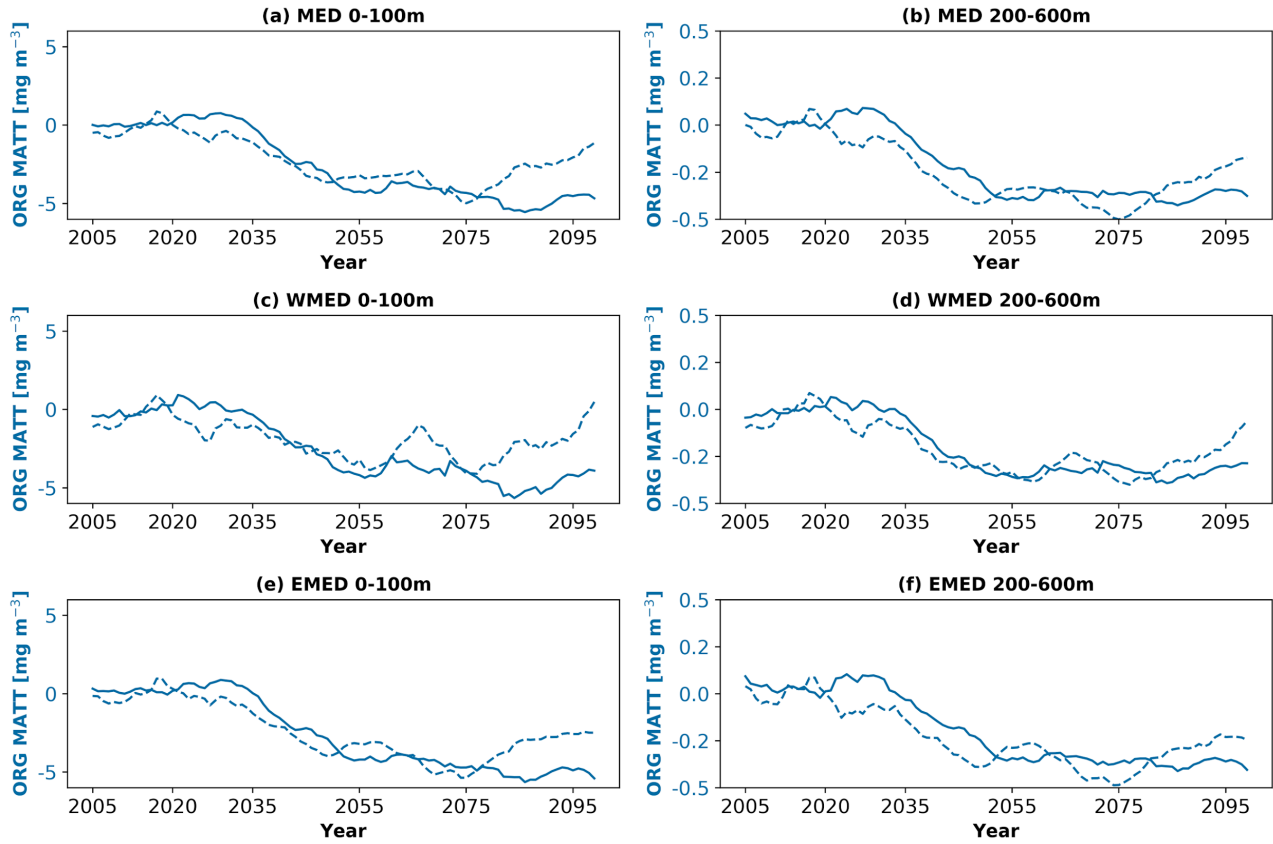
674

675 **Fig. 12 - Yearly time-series for the period 2005-2099 of Living/not Living organic Matter (in mg m^{-3}) anomalies for the emission**

676 **scenario RCP8.5 (solid line) and RCP4.5 (dashed line) in the Mediterranean Sea (MED, a-b), Western Mediterranean (WMED,**

677 **c-d) and Eastern Mediterranean (EMED, e-f) for the layer 0-100 m (left column) and 200-600 m (right column) for the 2005-**

678 **2099 period. The yearly time series have been smoothed using 10-years running mean.**

679

680
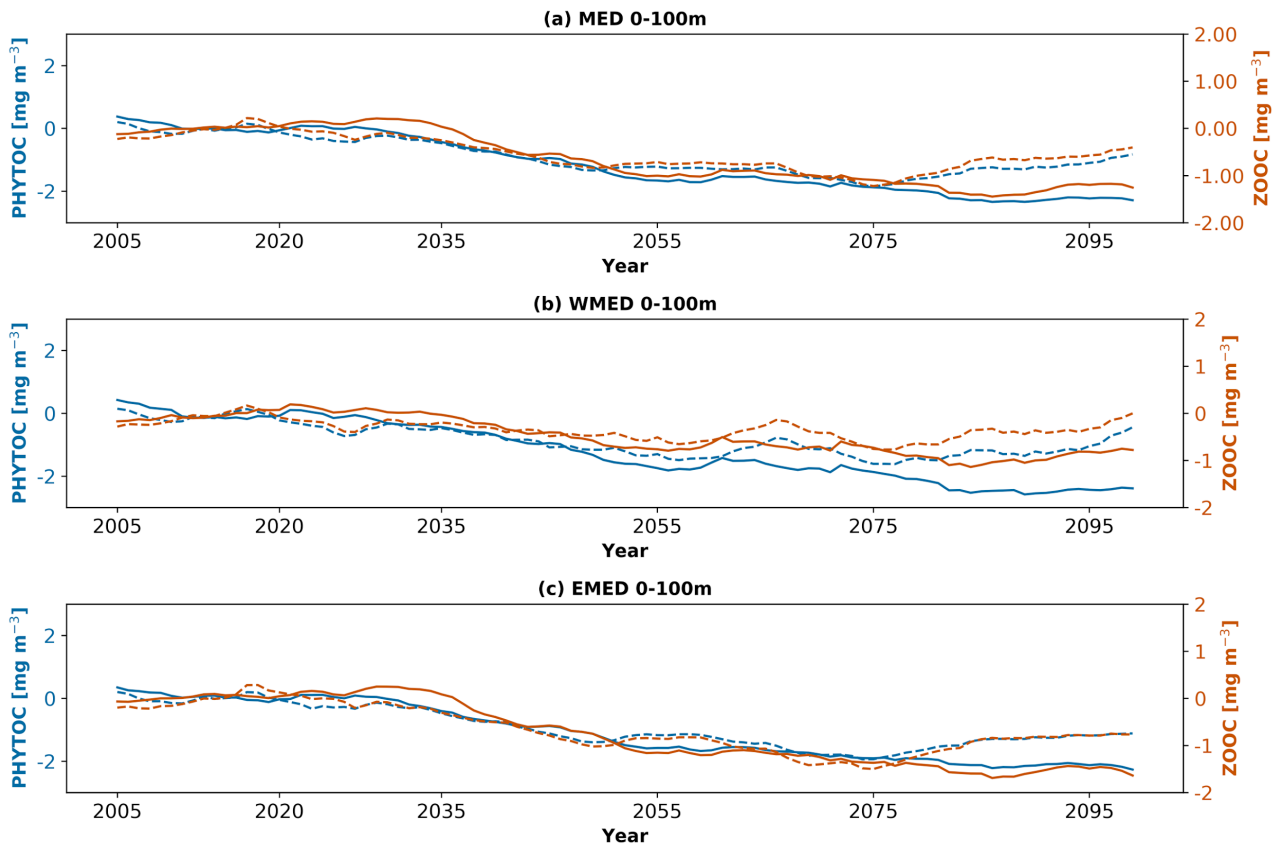
Fig. 13 - Yearly time series of Phytoplankton biomass (blue, in mg m⁻³) and Zooplankton (dark orange, in mg m⁻³) anomalies for the emission scenario RCP8.5 (solid line) and RCP4.5 (dashed line) in the Mediterranean Sea (MED, a), Western Mediterranean (WMED, b) and Eastern Mediterranean (c) for the layer 0-100 m and for the 2005-2099 period. The yearly time series have been smoothed using 10-years running mean.

In the two scenarios, in both MID-FUTURE and FAR-FUTURE, the areas most affected by the statistically significant decline of phytoplankton (Fig. S10) and zooplankton (Fig. S11) biomasses are mainly the sub-basins of the Eastern Mediterranean Sea, namely the Ionian Sea (mainly its Northern part), the Adriatic Sea (except for its Northern part), the Aegean Sea and the Levantine basin (in particular the Rhodes gyre area) and the Tyrrhenian Sea (only for the phytoplankton). Moreover, the negative anomaly in the area of Rhodes gyre is spatially coherent with the anomalies observed in the case of NPP and RESP, consequences of the vertical convection phenomena in the area. Conversely, positive but not statistically signals for both variables can be observed only at the local scale in the Strait of Sicily and along the coast of the North Western Mediterranean (spatially coherent with the positive variations of the PO₄ discussed in section 3.3 and in both cases not significant).
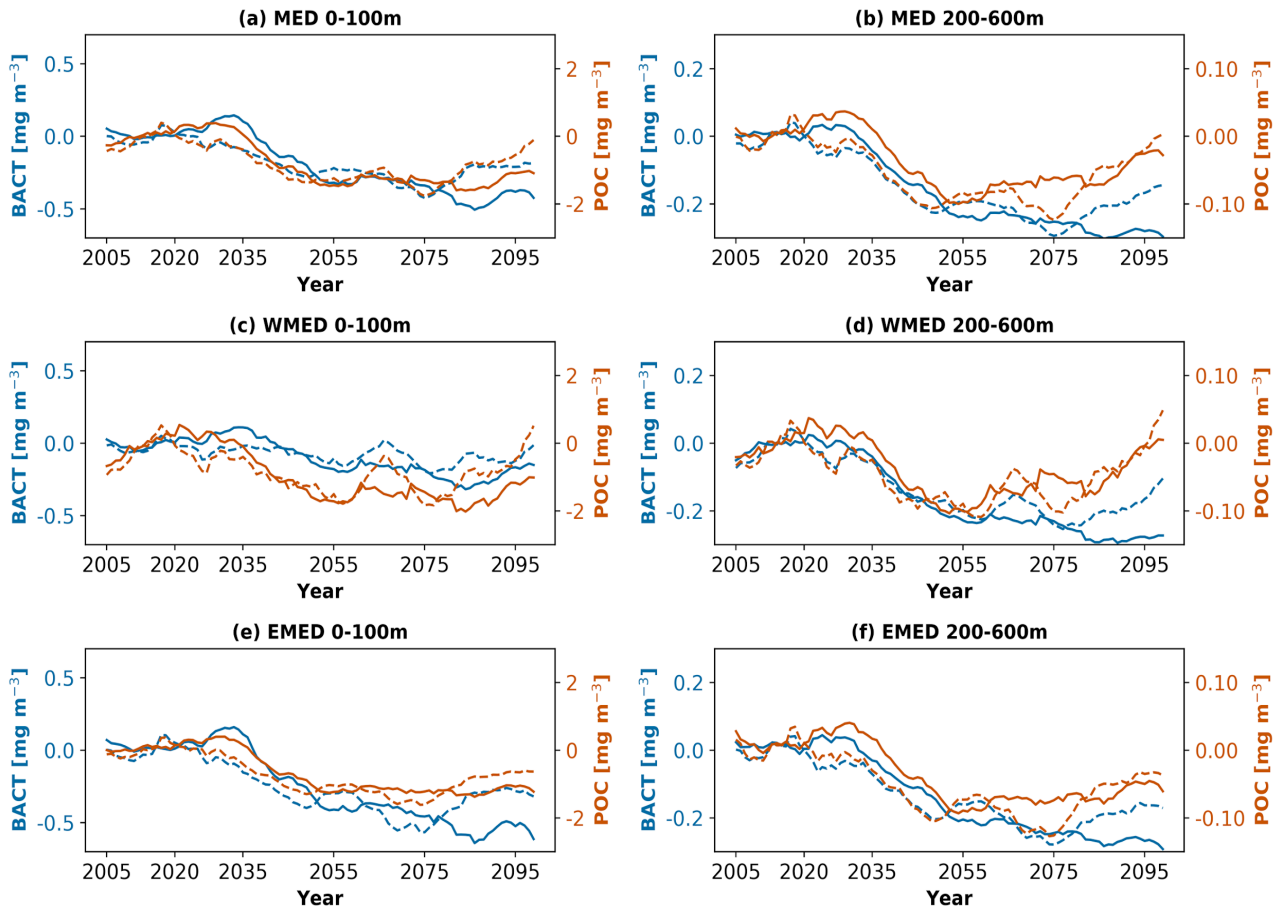
696

697 **Fig.14- As Fig.8 but for bacterial biomass (blue, in mg m⁻³) and particulate organic matter (dark orange, in mg m⁻³)**

698

699 Also in the case of bacterial biomass (Fig. S12) and particulate organic matter (Fig. S13) the decline, along the 21st

700 century, will mostly affect the euphotic and the intermediate layers of the Eastern basin, in both MID- and FAR-FUTURE,

701 with relative maxima observed in the Levantine basin (around 33.5% in RCP4.5 and 50% in the RCP8.5 scenario). This

702 decline is related to an increase of the respiration at community level, as observed for phytoplankton (Fig. S9). However,

703 there are some exceptions to the general decline of the bacterial biomass and particulate organic matter in the basin. For

704 example, in the Adriatic Sea, under scenario RCP8.5, the decrease of the bacterial biomass with respect to the beginning

705 of the century is only 1% with a slight positive anomaly appearing in the Southern Adriatic at the end of 21st century (not

706 statistically significant, Fig. S12). In the case of particulate organic matter, the Strait of Sicily and the Northern Adriatic

707 Sea are characterized by a permanent positive signal in both layers and scenarios as observed before for PO_4, also in this

708 case not statistically significant. Moreover, in RCP4.5 simulation, in the FAR-FUTURE period, the North Western

709 Mediterranean shows an increase of the particulate organic matter content in the euphotic and intermediate layers.

710

711 **3.4 Spatial and temporal evolution of dissolved inorganic carbon (DIC) and pH**

712

713 A basin-wide continuous increase in DIC is projected until the end of the 21st century, with a stronger signal observed in

714 the RCP8.5 scenario (Fig. 15), and more specifically, in the Eastern part of the Mediterranean basin. In fact, in the euphotic

715 layer, the increase in DIC with respect to the beginning of the century is approximately 150 μmol kg⁻¹ under RCP8.5 in

716 the Eastern basin, while it is approximately 120 μmol kg^{-1} in the Western basin. Additionally, in the intermediate layer,

717 DIC increases by approximately 120 μmol kg^{-1} with respect to the beginning of the century: this value is approximately

718 the same for both the Western and Eastern basins and is double with respect to that observed in the RCP4.5 scenario.

719
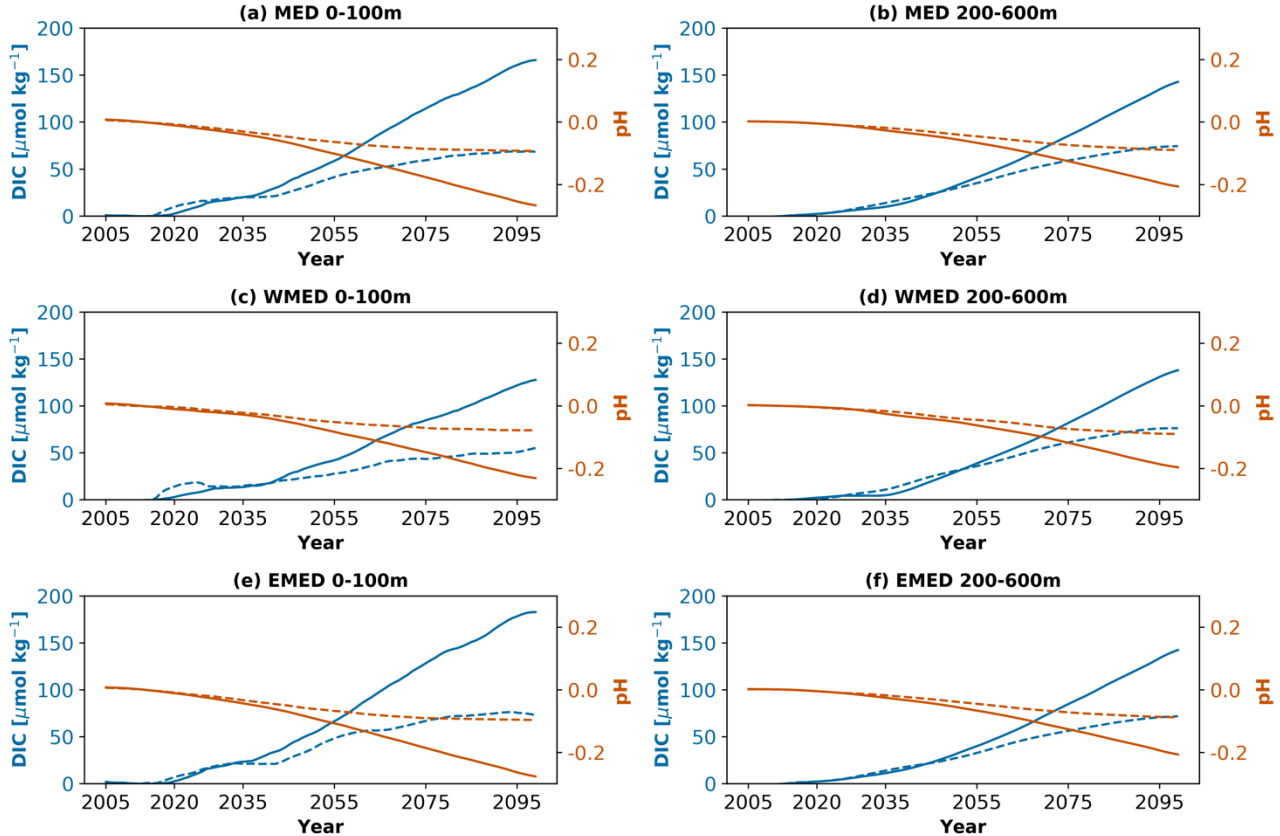
720

721

722 **Fig. 15 - as Fig.14 but for Dissolved Inorganic Carbon (blue, in μmol kg^{-1}) and pH (dark orange)**

723

724 Although community respiration can play a role in the increase in DIC, in the Mediterranean region a predominant

725 mechanism is represented by the air-sea CO_2 exchange (D'Ortenzio et al., 2008; De Carlo et al., 2013; Hassoun et al.,

726 2019; Wimart-Rousseau et al., 2020). In fact, looking at the terms controlling the DIC increase, the air-sea CO_2 exchange

727 shows an almost balanced condition in the present-day (D'Ortenzio et al., 2008; Melaku Canu et al., 2015), and an increase

728 throughout the 21st century as a consequence of the increase in atmospheric CO_2 (Fig. 16, a,b). The CO_2 flux increase is

729 almost linear and is equal in the two scenarios until 2050. Then, the RCP4.5 scenario shows a smoothing in the second

730 half of the century, which is consistent with the reduced atmospheric emissions, while the linear increase persists under

731 RCP8.5 (Fig. 16, a,b).

732

733 The two main Mediterranean sub-basins behave quite differently: the CO_2 air-sea sink is three times greater in the Western

734 part compared to the Eastern part, reflecting the influence of both DIC and temperature spatial gradients (i.e., higher

735 values of DIC and temperature in the Eastern basin). In order to assess the temperature and DIC contributions to the pCO$_2$

736 temporal evolution, the carbonate system equations of the BFM model have been solved in offline mode, keeping

737 constant, alternatively, temperature and DIC concentration. The increase in the temperature has been shown to account

738   for 25% of the total increase in the pCO_2. The remaining part of the pCO_2 increase can be ascribed to the DIC

739   concentration increase. In the Western part, a less pronounced temperature effect (i.e., temperature increases slower in

740   the Western part) causes an undersaturation condition of pCO_2 (i.e., pCO_2^{sea} lower than pCO_2^{atm} values) compared to the

741   Eastern conditions, triggering a much higher CO_2 absorption in the Western Mediterranean.

742
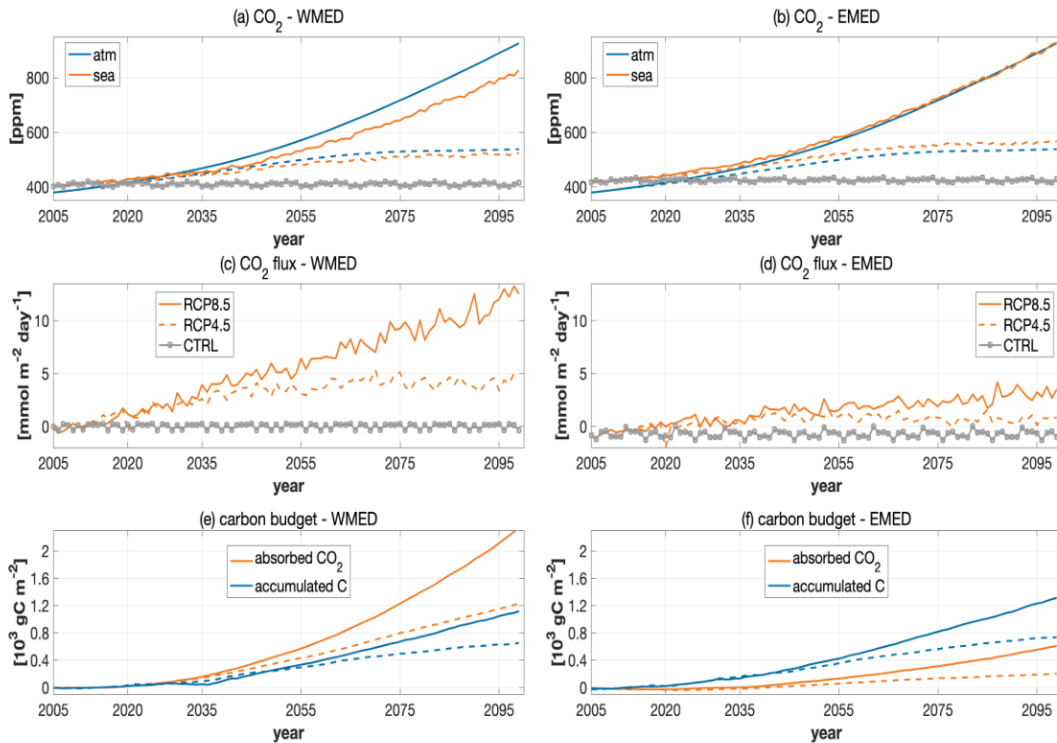
743

744

745   **Fig.16 - Time series of atmospheric and marine pCO_2 (a,b), CO_2 air-sea exchange (c,d) and cumulative CO_2 absorbed and**

746   **accumulated in the water column (e,f) in the Western (a,c,e) and Eastern (b,d,f) Mediterranean Sea. Two scenarios RCP4.5**

747   **(dashed line) and RCP8.5 (continuous line) and control simulation (CTRL, gray line) are reported.**

748

749   As a result of the air-sea CO_2 sink, for example the RCP8.5 scenario shows a steady DIC accumulation after 2030 with

750   values of more than 2 μmol kg^{-1} year^{-1} in the first 600 m (500 m) of the water column for the Western basin (Eastern

751   basin; Fig. 17).

752

753   The increase in DIC in the upper layer is approximately 1.5% and 2.5% in the Western and Eastern basins, respectively,

754   in the MID-FUTURE, and 5% and 7% in the FAR-FUTURE (Fig. S14). In the 200-600 m layer, the DIC increase follows

755   the same pattern as that in the upper layer, but with smaller changes (i.e., approximately 1-2% less). Then, while the DIC

756   increase does not impact the water column below 1200 m in the Western basin, DIC still accumulates until 2000 m in the

757   Eastern basin at a rate of almost 0.5 μmol kg^{-1} year^{-1} (Fig. 17). Occasional events of deep transport of DIC can be

758   recognized (e.g. around the years 2035, 2045, 2085 and 2095, similar to what observed in the case of oxygen in Fig.9)

759   and the water column results enriched down to 1000-1500 m with a rate of approximately 1 μmol kg^{-1} year^{-1}. In the surface

760   layer (i.e., first 50-100 m), the interannual variability of atmospheric conditions (i.e. specific annual wind and temperature

761 seasonal cycles triggering the CO_2 fluxes) and the winter mixing produce an irregular succession of positive and negative
762 annual changes, which can partially hide the long-term effect of the increase in atmospheric pCO_2. Thus, the cumulative
763 sum of the CO_2 absorbed through air-sea exchanges and of the carbon accumulated in the water column (Fig. 16, e,f)
764 highlight the different behavior of the two main sub-basins. The Western basin absorbs much more atmospheric CO_2 than
765 the Eastern basin, with even larger differences in the RCP8.5 scenario. By the end of the RCP8.5 scenario, 1.8 PgC of
766 atmospheric CO_2 sink in the Western basin while only 1 PgC in the Eastern basin are observed, consistent with the
767 estimates of Solidoro et al. (2022).
768
769 However, the fate of the absorbed carbon is quite different: the Western basin during the 21st century (RCP8.5 scenario)
770 accumulates only 0.85 PgC, while 1.7 PgC are retained in the water column of the Eastern basin. As shown in Figure 16
771 (lower panel) for the RCP8.5 scenario, the Eastern basin accumulates almost 2 moles of carbon for each atmospheric CO_2
772 mole absorbed (up to 3 in the RCP4.5), while it is less than 0.5 for the Western basin. The different efficiency is eventually
773 triggered by the thermohaline circulation change: the Western Mediterranean carbon is partly exported to the Northern
774 Atlantic Ocean, while an increased quota of carbon input from rivers and across the Sicily channel are retained in the
775 Eastern basin together with the atmospheric CO_2 sink after the weakening of the thermohaline circulation (Fig.4). The
776 RCP4.5 scenario shows similar dynamics to RCP8.5, with rates of CO_2 absorption (Fig. 16) and of DIC accumulation
777 almost halved, and the impact of the interannual variability on surface layer dynamics much more amplified (not shown).
778 As a result, the total sequestered atmospheric CO_2 equals to 0.8 and 0.25 PgC in the Western and Eastern basins, while
779 the increases of the carbon pool are 0.5 PgC and 0.9 PgC, respectively.
780

781
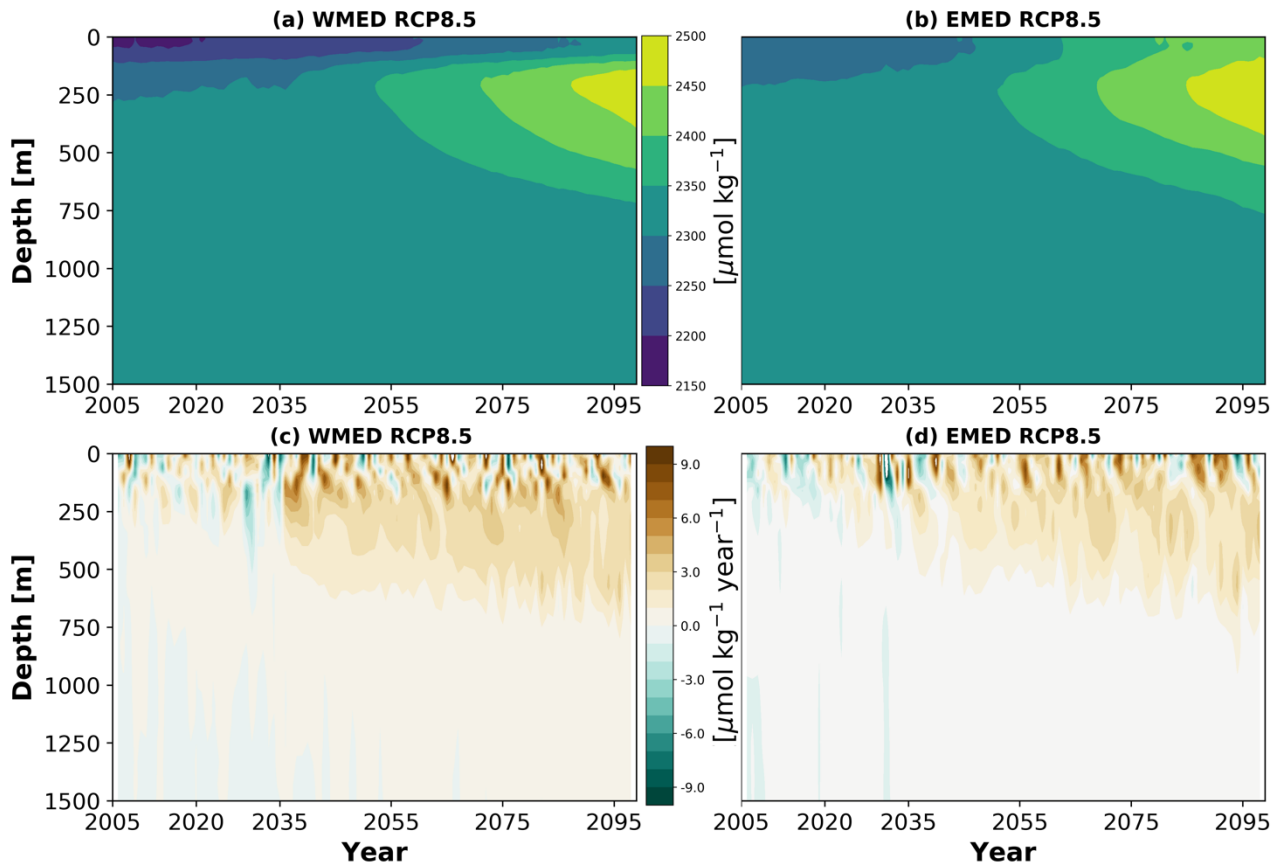
Fig. 17 - Hovmoeller diagram of DIC (µmol kg^{-1}, panel a,b) and annual rate of change of DIC (µmol kg^{-1}year^{-1}, panel c,d) in the Western (a,c) and Eastern (b,d) Mediterranean Sea in RCP8.5 scenario.

Consequently, to the CO_2 invasion and DIC increase, the change in the carbonic acid equilibrium causes a generalized decrease in pH, as also shown in Solidoro et al. (2022) in the case of the A2 scenario. The change in pH, which is statistically significant everywhere and very well anti-correlated in time and space with the DIC change (on the basin scale the correlation coefficient is lower than -0.90 with p<0.05; Fig.S14) and almost similar in both Western and Eastern Mediterranean (as already projected by Goyet et al, 2016), is approximately by the end of the century equal to 0.1 in the RCP4.5 and 0.25 pH units in the RCP8.5 scenario (Fig. 18). The largest decreases in pH are projected in both scenarios in the upper layer of the North-Western Mediterranean, Tyrrhenian Sea, Adriatic Sea and Aegean Sea and in the 200-600 m layers of the Tyrrhenian Sea, Ionian Sea and Aegean Sea in the FAR-FUTURE (Fig. 18).

pH
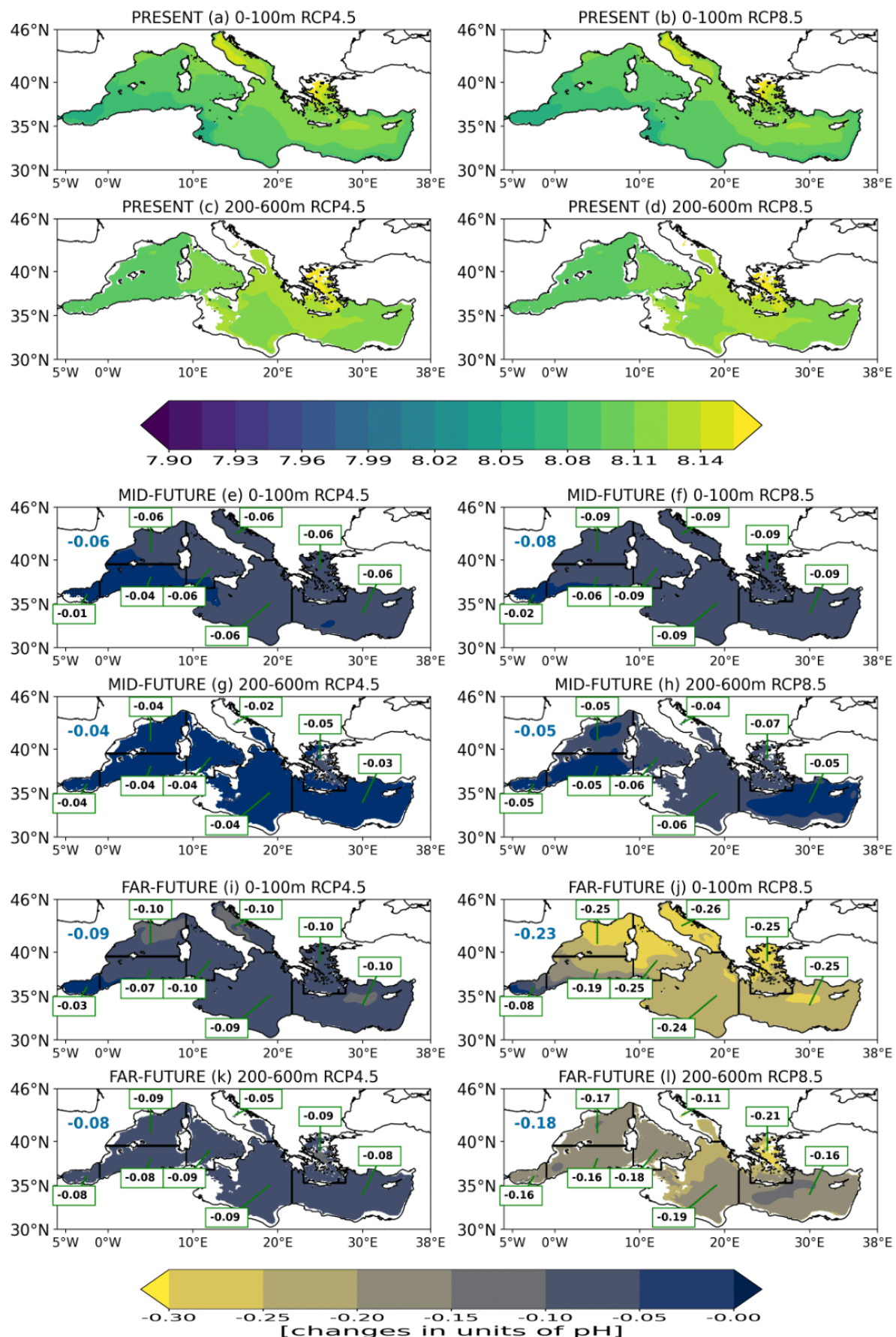
794 **Fig. 18 –pH in the layers 0-100 m and 200-600 m in the PRESENT (2005-2020, a,b,c and d), and relative climate change signal**

795 **(with respect to the PRESENT, in units of pH) in the MID-FUTURE (2040-2059, e,f,g and h) and FAR-FUTURE (2080-2099,**

796 **i,j,k and l) in the RCP4.5 (left column) and RCP8.5 (right column) scenarios. The Mediterranean average relative climate**

797 **change signal in each period (with respect to the PRESENT) is displayed by the top-left colored value (blue or dark orange**

798 **when negative or positive). Values in the green boxes is the average relative climate change signal in each period and in each**

799 **sub-basin shown in Figure 1. Domain grid points where the relative climate change signals are not statistically significant**

800 **according to a Mann-Whitney test with p<0.05 are marked by a dot.**

801

802

803

804 **4. Discussions and Conclusions**

805

806 In this study, the coupled physical-biogeochemical model MFS16-OGSTM-BFM is used to simulate the biogeochemical

807 dynamics of the Mediterranean Sea during the 21st century under the two emission scenarios RCP4.5 and RCP8.5, and

808 to assess some climate-related impacts on the marine ecosystems of the basin.

809

810 To the best of the authors' knowledge, this work is the first one that analyzes long-term eddy-resolving projections of the

811 biogeochemical dynamics of the Mediterranean Sea under two different emission scenarios. In fact, the horizontal and

812 vertical resolution (1/16° and 70 vertical levels) of the long-term projections here analyzed is higher than that of previous

813 works available in the scientific literature that focuses on the area (e.g Lazzari et al., 2014; Macias et al., 2015; Richon et

814 al., 2019; Pagès et al., 2020; Solidoro et al., 2022). Moreover, the majority of the recent scientific works discussing the

815 impacts of climate change on the biogeochemical dynamics of the Mediterranean Sea are based on the analysis of

816 simulation that considered the worst-case emission scenario (A2 or RCP8.5; Moullec et al., 2019; Richon et al., 2019;

817 Pagés et al., 2020; Solidoro et al., 2022).

818

819 The use of eddy-resolving resolution and of a higher vertical resolution allows a more detailed representation of the

820 vertical mixing and ocean convection processes, which play a fundamental role in the ventilation of the water column and

821 in the nutrient supply into the euphotic layer of the basin (Kwiatkowski et al., 2020). Moreover, the use of a 1/16°

822 horizontal resolution for the projections has allowed to resolve, identify and characterize, for the first time, spatial

823 gradients existing in the same sub-basins (such as in the Adriatic Sea) or between coastal and open ocean areas (such as

824 in the North Western Mediterranean). A more detailed representation of the spatial distribution of the projected changes

825 and of their statistical significance for different biogeochemical tracers and properties represents a clear advantage for the

826 future assessment of climate change impacts on specific organisms, habitats or target areas, also at sub-basin scale.

827

828 The analysis of the thermohaline properties and circulation of the Mediterranean Sea under emission scenarios RCP4.5

829 and RCP8.5 found different levels of warming of the water column and weakening of the thermohaline circulation cell,

830 with different parts of the basin being characterized by contrasting saltening and freshening conditions as a function of

831 the considered scenario. Moreover, different levels of weakening of the open ocean convection in the most important

832 convective areas of the basin are projected, with the only exception of the Aegean Sea, where episodes of deep convection

833 similar to the EMT could be observed at the end of the 21st century (see also Adloff et al., 2015). All the projected

834   changes are in agreement with those already depicted in recent model studies (e.g. Somot et al., 2006; Adloff et al., 2015;

835   Waldman et al., 2018; Soto-Navarro et al., 2020).

836

837   A comparison of the model outputs with available data in the present climate, together with previous studies performed

838   with the same model system, support the conclusion that the coupled model MFS16-OGSTM-BFM has a reasonably good

839   ability in reproducing the main biogeochemical features of the Mediterranean Sea and can be used as a tool for assessing

840   the future biogeochemical dynamics of the basin and its changes in response to climate change. The use of the bias-

841   removing protocol is often advocated as a good practice in climate studies, but rarely implemented in biogeochemical or

842   ecosystem projections (e.g., Solidoro et al., 2022) and it adds further robustness to our results.

843

844   Our projections for the biogeochemical tracers and properties at the end of the 21st century shows several signals (see

845   Table SP1 for a synthetic overview) that are mostly in agreement with previous studies, at least with those based on the

846   use of the worst-case emission scenarios. The magnitude of the projected changes has been shown to be, in general,

847   scenario-dependent with the largest deviations from the present climate state observed in the RCP8.5 emission scenario

848   (Table SP1). On the other hand, the analysis of the projections under RCP4.5 found in most of the biogeochemical

849   variables (for example dissolved nutrients and biomasses) by the end of the 21st century a tendency to recover the values

850   observed in the present climate (Table SP1).

851

852   As shown in the previous sections, our simulations, by covering also the RCP4.5 scenario, highlight how an intermediate

853   greenhouse emission scenario produces results that are not simply an average between the present condition and the

854   RCP8.5, but (at least for some variables) something quantitatively different. For example, the temporal evolution of pH

855   (Fig.15) is similar in two scenarios in the first 30 years of the 21st century. Conversely, after 2050, pH undergoes a

856   substantial decrease under RCP8.5 while it remains almost stable under RCP4.5 with a final projected variation lower

857   than the half with respect to the worst-case scenario. This supports the idea - possibly based on the existence of a certain

858   buffer capacity and renewal rate in a system like the Mediterranean Sea - that the implementation of policies of reducing

859   CO_2 emission could be, indeed, effective and could contribute to the foundation of ocean sustainability science and

860   policies.

861

862   The decline in the dissolved nutrients at the surface under RCP8.5 scenario is comparable with that observed in Richon

863   et al. (2019). However, they project an overall increase in the concentration of both nutrients at the surface after 2050,

864   which is ascribed by the authors to river and Gibraltar inputs that are not constant over time (as in our case) but are based

865   on a global climate scenario simulation. As highlighted by Richon et al. (2019), the sensitivity of the biogeochemical

866   fluxes at the river loads and Gibraltar exchanges is of paramount importance, and surely worthy of further investigation.

867   Nevertheless, the increase in the concentration of nutrients in the intermediate layers of both the Western Mediterranean

868   and Levantine basin can be also traced back to the reduced vertical mixing resulting from the increase in the vertical

869   stratification (Somot et al., 2006; Adloff et al., 2015; Richon et al., 2019).

870

871   Different levels of increase in the net primary production and respiration are projected in both scenarios although many

872   recent studies in the Mediterranean region have shown a different response of integrated net primary production to climate

873   change in both Western and Eastern basins (e.g. Macias et al., 2015; Moullec et al., 2019; Pagès et al., 2020). In fact, this

874   response may vary according to the sensitivity of the assumptions (model equations) for primary production and recycling

875 processes to changes in temperature (Moullec et al., 2019). In the BFM model temperature regulates most of the metabolic
876 rates with a Q10 formulation (Vichi et al., 2015). The increase in net primary production is a consequence of such
877 dependence. In other studies (Eco3M-Med model; Pages et al., 2020) organisms are always optimally adapted and no
878 temperature dependence is accounted for in the physiology. This different parameterization could be connected to the
879 different results in terms of trends; in fact, the scenarios based on the Eco3M-Med model results in a reduction of net
880 primary production. In this case surface nutrient reduction, rather than temperature, affects the net primary production
881 trend producing a decrease. The relative impact of different drivers (nutrient supply versus organism's adaptation to
882 average water temperature) could be explored with dedicated sensitivity experiments.

884 Our projections of net primary production and biomass dynamics show how different levels of warming of the water
885 column and consequent stratification have a direct impact on the ecosystem functioning by increasing the metabolic rates.
886 Similar to the results obtained in Lazzari et al. (2014) and Solidoro et al. (2022), the increase in metabolic rates augments
887 both primary production and respiration, but with the net effect of reducing living and non-living particulate organic
888 matter, as suggested from theoretical considerations in O'Connor et al. (2011). The decoupled formulation of carbon
889 uptake and net growth in the BFM model induces a further mechanism related to how carbon is channeled in the food
890 web. In fact, the decrease in biomass is partially compensated by an increase in dissolved organic matter production in
891 the basin by the end of the century (Solidoro et al., 2022; results not shown here).

893 Basin-wide deoxygenation tendencies are found in both scenarios and are comparable to trends observed on the
894 Mediterranean scale by Powley et al. (2018) and, under RCP8.5, on the global scale by CMIP6 simulations (Coupled
895 Model Intercomparison Project Phase 6; Kwiatkowski et al., 2020). The former, using a box model, found a decrease in
896 the oxygen content of the intermediate layer in the range of 2-9% as a consequence of different projected changes in the
897 solubility (due to the temperature increase) and in the thermohaline circulation of the basin. Furthermore, the projections
898 show that, in both our scenarios, deoxygenation is higher in the Eastern than the Western basin, where the Atlantic
899 boundary condition might have dumped the deoxygenation trend, and in several coastal areas such as the Northern
900 Adriatic (until -25 mmol m^{-3}). As also observed by Powley et al. (2018), the main driver of deoxygenation is the change
901 in solubility, whereas changes in the circulation (i.e., weakening of the thermohaline circulation) should not substantially
902 affect deep ventilation, and it is unlikely, even in the worst-case scenario, to reach hypoxia conditions in the deep layer
903 of the basin by the end of the century. On the other hand, the greatest threat for the oxygen water content might be linked
904 to the combination of surface warming and faster respiration processes in the coastal areas of the basin which could result
905 in lower oxygen conditions and, thus, alteration of the local marine ecosystem functioning and structures (Bindoff et al.,
906 2019).

908 An increase in the dissolved inorganic carbon content and acidity of the water column (Solidoro et al., 2022) is found in
909 both scenarios. The overall accumulation of CO_2 in the basin resulted in an acidification of the Mediterranean water with
910 a decrease in pH of approximately 0.23 units in the worst-case scenario, which is slightly lower than the 0.3 projected on
911 a global scale (Kwiatkowski et al., 2020) and lower than the value provided in Goyet et al. (2016), who projected, using
912 thermodynamic equations of the CO_2/carbonate system chemical equilibrium in seawater, a variation of 0.45 pH units in
913 the basin under the worst SRES case scenario (and 0.25 pH units in the most optimistic SRES scenario). However, this
914 last estimate probably tends to overestimate the future acidification of the basin, as it does not consider the decrease in

915   the exchanges and the penetration of CO_2 across the ocean-atmosphere interface due to the warming of the water column

916   (MedECC, 2020).

917   This difference in the response to climate change between the Western and Eastern basins has been also observed for the

918   dissolved inorganic carbon accumulation and reflects indeed different factors such as the different ventilation and

919   residence time of water masses in the two basins as well as the exchanges in the Strait of Gibraltar (e.g. Alvarez et al.,

920   2014; Stöven and Tanhua, 2014; Cardin et al., 2015; Hassoun et al., 2015). Results show that, in both scenarios, the

921   Western basin, while adsorbing greater quantities, accumulates only a half of the atmospheric carbon stored by the Eastern

922   basin because in the former the carbon is partly exported to the Northern Atlantic Ocean, while in the latter, it is also

923   affected by a more intense reduction of the thermohaline circulation and therefore in the vertical transport processes, the

924   carbon is retained together with the atmospheric CO_2 sink. Additionally, in our case, the use of a high resolution for the

925   biogeochemical projections has allowed to show that in many coastal areas the observed acidification is lower by

926   approximately 8% with respect to the open ocean due to damping effects of ALK input from the rivers (not shown here).

927   The decline in many biogeochemical tracers and properties in the euphotic layer begins in the 2030-2035 period, in

928   correspondence to the weakening of the thermohaline circulation in the basin (Fig. 4), and it is particularly marked in the

929   Eastern basin. This shows that the modification of the circulation resulting from future climate scenarios has substantial

930   effects on the biogeochemical properties of the basin. Changes in the thermohaline circulation of the basin also explain

931   the increase in the nutrient concentration in the intermediate layer of the Levantine basin, which is a result of the

932   weakening of the westward transport of nutrients through the Strait of Sicily (Fig.S5).

933

934   Similar to all previous modelling cited studies (e.g Lazzari et al., 2014; Macias et al., 2018; Richon et al., 2019; Pagès et

935   al., 2020), some sources of uncertainties for our projections need to be considered. As discussed before, MFS16

936   adequately reproduces the distribution of key physical properties and the thermohaline circulation of the basin. On the

937   other hand, recent studies based on multi-model ensembles (Adloff et al., 2015; Richon et al., 2019; Soto-Navarro et al.,

938   2020) have suggested that atmospheric forcing and boundary conditions can strongly affect the dynamics of the basin,

939   particularly the vertical mixing, which plays a primary role in the distribution of nutrients in the euphotic layer, therefore

940   affecting the dynamics of low trophic levels. Additional sources of uncertainties in the modelling framework can be traced

941   back to the BFM biogeochemical model. For instance, in the present climate the model tends to overestimate the chl-*a* at

942   the surface and, even more, the oxygen concentration below 200 m (section 3.1). These overestimations can be propagated

943   by the integration into the future projections. However, the conclusions of the present work should not be significantly

944   affected by that because, at the same time, the CTRL simulation is also removed from both the scenario simulations.

945   Moreover, the signs of the projected changes (not their absolute values) result from different physical and biogeochemical

946   processes (e.g., temperature and respiration increase, weakening of the thermohaline circulation, increase in the

947   stratification) which are linked to the climate forcing and are independent from model uncertainties that generate the

948   biases discussed in section 3.1.

949

950   Furthermore, the set-up of the boundary conditions, namely the atmospheric deposition at the surface, the rivers nutrient

951   loads and the vertical profiles in the Atlantic boundary can be very critical, especially in the land-locked Mediterranean

952   basin. Atmospheric deposition is an important source of nutrients for the basin and it has been shown that the

953   biogeochemical dynamics of the Mediterranean Sea is influenced by aerosol deposition (e.g. Richon et al., 2018, 2019),

954 especially during periods of stratification. The projected lower nutrient supply from sub-surface waters caused by climate-

955 driven stronger stratification, could likely increase the importance of the atmospheric deposition as a source of nutrients

956 for the euphotic layer (Gazeau et al., 2021). Thus, possible future changes in the deposition of aerosols could influence

957 the biogeochemistry of the basin and the nutrients concentration at the surface as projected for the 21st century and

958 depicted in Section 3.3. However, in both RCP4.5 and RCP8.5 simulations, a present-day phosphate and nitrogen

959 deposition is used. Potential improvements will be achieved indeed by the inclusion of more accurate deposition

960 information derived from CMIP6 global estimates for the 21st century (O'Neill et al., 2016).

961

962 Similarly, the lack of river nutrient load projections under the prescribed emission scenarios can affect the projected

963 nutrient budget of the Mediterranean basin. A climatology derived from the Perseus project (see Section 2.3) is here

964 adopted, which is, to our knowledge, the most reliable information. Indeed, it is reasonable to assume that land-use and

965 runoff changes might impact future nutrient loads, although the magnitude and even the sign are presently unknown. Our

966 river runoff was based on projections (Gualdi et al., 2013; Section 2.1) which estimated an average decrease by the end

967 of the 21st century. Thus, the increase of nutrients observed in Fig. 9 and Fig. 10 in the Northern Adriatic and several

968 coastal areas of the Western basin can be partially related to the mismatch between a constant nutrient load and a

969 decreasing runoff. However, it might be worth remembering that the amount of nutrients entering the basin through its

970 boundaries ultimately depends on the economic policies and land use/coverage scenarios and therefore they may be

971 intrinsically subjective.

972

973 With DIC as the only exception, for the 21st century, a single vertical profile based on the present-day condition data is

974 used and no future evolutions are considered for the boundary conditions at the Strait of Gibraltar. If this approach allows

975 to point out the effects of the changes in the basin circulation on the nutrient budgets, it could miss the influence on

976 nutrients or other biogeochemical properties of a possible different future evolution of the exchanges in the Strait of

977 Gibraltar due to changes in the tracer concentrations in the Atlantic Ocean. Moreover, the use of the same Atlantic

978 boundary conditions for the two scenarios (section 2.3) could have led to an underestimation of a potential difference

979 between the two scenarios in the areas most influenced by the Atlantic boundary (e.g. Alboran Sea and South Western

980 Mediterranean). Recent physical simulations have shown an increase of 3.7% in the surface flow at the Strait of Gibraltar,

981 which could imply an increase in the inflow of nutrients in the surface layer at Strait of Gibraltar (Richon et al., 2019;

982 Pagès et al., 2020), thereby eventually damping the decrease in the nutrient concentration at the surface projected for the

983 21st century. As previously observed, this could explain the observed differences among different studies that analysed

984 future projections of the biogeochemistry of the basin.

985

986 To conclude, the methodology and results here presented, provide a robust picture of the evolution of the Mediterranean

987 Sea biogeochemistry for the 21st century. Clearly, the new generation of Regional Earth System Coupled Models

988 (RESM), with eddy-resolving ocean models such as the one exploited here, may partially reduce the limitations of using

989 external (and possibly misaligned) sources of information for atmospheric and land input to the ocean. Indeed, by directly

990 resolving the coupling between the Mediterranean Sea, the regional atmospheric domain and the hydrological component,

991 a regional earth system coupled model (e.g., as in Sitz et al., 2017, and Reale et al., 2020a) allows the simulation of the

992 different components of the climate system at the local scale, including aerosol and river loads.

993

994 **Acknowledgements**

M. Reale has been supported in this work by OGS and CINECA under HPC-TRES award number 2015-07 and by the project FAIRSEA (Fisheries in the Adriatic Region - a Shared Ecosystem. Approach) funded by the 2014 - 2020 Interreg V-A Italy - Croatia CBC Programme (Standard project ID 10046951). This work has been partially supported by the Italian PRIN project ICCC (Impact of Climate Change on the biogeochemistry of Contaminants in the Mediterranean Sea). The CINECA consortium is acknowledged for providing the computational resources through the IscraB project "Scenarios for the Mediterranean Sea biogeochemistry in the 21st century" (MED21BIO) and the IscraC DYBIO, EMED18 and MEDCLI16. This study has been conducted also using E.U. Copernicus Marine Service Information. The authors acknowledge Dr. Abed El Rahman Hassoun, an anonymous Reviewer and the Associate Editor Jean-Pierre Gattuso for providing suggestions and criticisms that greatly improved the study.

Data availability

Data produced in the numerical experiments are available through the portal dds.cmcc.it for both physical (https://dds.cmcc.it/#/dataset/medsea-cmip5-projections-physics) and biogeochemical (https://dds.cmcc.it/#/dataset/medsea-cmip5-projections-biogeochemistry) components.

Author contribution

GC, PL, SS, MR and CS conceived the study. They designed the experiments together with TL. MR, GB and TL performed the numerical simulations. MR, GC, SS, TL and PL performed the analysis of the simulation results. MR prepared the first draft of the manuscript under the supervision of SS, GC, PL and CS and with the contribution from all the authors. All the authors discussed the results and contributed to the revision of the manuscript.

Competing interest

The authors declare that they have no competing interests.

References

Álvarez, M., Sanleón-Bartolomé, H., Tanhua, T., Mintrop, L., Luchetta, A., Cantoni, C., Schroeder, K., and Civitarese, G.: The CO_2 system in the Mediterranean Sea: a basin wide perspective, Ocean Sci., 10, 69–92, https://doi.org/10.5194/os-10-69-2014, 2014.

Adloff, F., Somot, S., Sevault, F., Jordà, G., Aznar, R., Déqué, M, Herrmann, M., Marcos, M., Dubois, C., Padorno, E., Alcarez-Fanjul, E., Gomis, D.: Mediterranean Sea response to climate change in an ensemble of twenty first century scenarios. *Clim Dyn* 45, 2775–2802. https://doi.org/10.1007/s00382-015-2507-3, 2015.

Auger, P.A., Ulses, C., Estournel, C., Stemman, L., Somot, S. and Diaz, F.: Interannual control of plankton ecosystem in a deep convection area as inferred from a 30-year 3D modeling study: winter mixing and prey/predator in the NW Mediterranean. Progress in Oceanography, 124, 12-27, DOI: 10.1016/j.pocean.2014.04.004, 2014.

1033 Benedetti, F., Guilhaumon, F., Adloff, F. and Ayata, S.D: Investigating uncertainties in zooplankton composition shifts
1034 under climate change scenarios in the Mediterranean Sea. Ecography, 41: 345-360. https://doi.org/10.1111/ecog.02434,
1035 2018.

1036

1037 Bethoux, J. P., Morin, P., Chaumery, C., Connan, O., Gentili, B., and Ruiz-Pino, D.: Nutrients in the Mediterranean Sea,
1038 mass balance and statistical analysis of concentrations with respect to environmental change, Mar. Chem., 63, 155–169,
1039 1998.

1040 Bindoff, N.L., Cheung, W.W.L., Kairo, J.G., Arístegui, J., Guinder, V.A., Hallberg, R., Hilmi, N., Jiao, N., Karim, M.S.
1041 , Levin, L., O'Donoghue,S., Purca Cuicapusa, S.R. , Rinkevich,B., Suga, T., Tagliabue,A., and Williamson, P.: Changing
1042 Ocean, Marine Ecosystems, and Dependent Communities. In: *IPCC Special Report on the Ocean and Cryosphere in a*
1043 *Changing Climate* [H.-O. Pörtner, D.C. Roberts, V. Masson-Delmotte, P. Zhai, M. Tignor, E. Poloczanska, K.
1044 Mintenbeck, A. Alegría, M. Nicolai, A. Okem, J. Petzold, B. Rama, N.M. Weyer (eds.)], 477-587, 2019.

1045

1046 Buga, L., Sarbu,G., Fryberg,L., Magnus, W., Wesslander,K., Gatti, J., Leroy,D., Iona,S., Larsen, M., Koefoed Rømer,
1047 J., Østrem, A.K., Lipizer, M., Giorgetti, A.: EMODnet Thematic Lot n° 4/SI2.749773 EMODnet Chemistry
1048 Eutrophication and Acidity aggregated datasets v2018 doi: 10.6092/EC8207EF-ED81-4EE5-BF48-E26FF16BF02E,
1049 2018.

1050

1051 Butenschön, M., Lovato, T., Masina, S., Caserini, S., and Grosso, M.: Alkalinization Scenarios in the Mediterranean Sea
1052 for Efficient Removal of Atmospheric CO2 and the Mitigation of Ocean Acidification. *Frontiers in Climate*, *3*, 14 ,2021.

1053

1054 Canu, D. M., Ghermandi, A., Nunes, P. A., Lazzari, P., Cossarini, G., and Solidoro, C.: Estimating the value of carbon
1055 sequestration ecosystem services in the Mediterranean Sea: An ecological economics approach. *Global Environmental*
1056 *Change*, *32*, 87-95, 2015.

1057

1058 Cardin, V., Civitarese, G., Hainbucher, D., Bensi, M., and Rubino, A.: Thermohaline properties in the Eastern
1059 Mediterranean in the last three decades: is the basin returning to the pre-EMT situation?, Ocean Sci., 11, 53–66,
1060 https://doi.org/10.5194/os-11-53-2015, 2015.

1061

1062 Claustre, H., Morel, A., Hooker, S. B., Babin, M., Antoine, D., Oubelkheir, K., Bricaud, A., Leblanc, K., Quéguiner, B.,
1063 Maritorena, S.: Is desert dust making oligotrophic waters greener? Geophys. Res. Lett., 29, 1–4,
1064 https://doi.org/10.1029/2001GL014056, 2002.

1065 Colella, S., Falcini, F., Rinaldi, E., Sammartino, M., and Santoleri, R.: Mediterranean Ocean colour chlorophyll trends.
1066 *PLoS ONE*, 11(6), e0155756. https://doi.org/10.1371/journal.pone.0155756, 2016.

1067 Cossarini, G., Lazzari, P., Solidoro, C.: Spatiotemporal variability of alkalinity in the Mediterranean Sea, Biogeosciences,
1068 12, 1647-1658, https://doi.org/10.5194/bg-12-1647-2015, 2015.

1069

1070 Cossarini G, Feudale L, Teruzzi A, Bolzon G, Coidessa G, Solidoro C, Di Biagio V, Amadio C, Lazzari P, Brosich A and
1071 Salon S High-Resolution Reanalysis of the Mediterranean Sea Biogeochemistry (1999–2019). Front. Mar. Sci. 8:741486.
1072 doi: 10.3389/fmars.2021.741486, 2021

1073

1074 Crise, A., Allen, J., Baretta, J., Crispi, G., Mosetti, R., Solidoro, C.: The Mediterranean pelagic ecosystem response to
1075 physical forcing Progress in Oceanography 44 (1-3), 219-243, 1999.

1076

1077 Crispi, G., Mosetti, R., Solidoro, C., Crise, A.: Nutrient cycling in Mediterranean basins: the role of the biological pump
1078 in the trophic regime Ecol. Model.,138pp.101-114, 2001.

1079

1080 Darmaraki, S., Somot, S., Sevault, F., Nabat P., Cabos Narvaez W.D., Cavicchia L., Djurdjevic V., Li L, Sannino G.,
1081 Sein D.V: Future evolution of Marine Heatwaves in the Mediterranean Sea. *Clim Dyn* **53,** 1371–1392.
1082 https://doi.org/10.1007/s00382-019-04661-z, 2019.

1083

1084 De Carlo, E.H., Mousseau, L., Passafiume, O., Drupp, P., Gattuso, J.P.: Carbonate Chemistry and Air–Sea CO_2 Flux in a
1085 NW Mediterranean Bay Over a Four-Year Period: 2007–2011. *Aquat Geochem* **19,** 399–442
1086 https://doi.org/10.1007/s10498-013-9217-4, 2013.

1087

1088 Di Biagio, V., Cossarini, G., Salon, S., Lazzari, P., Querin, S., Sannino, G., Solidoro, C.: Temporal scales of variability
1089 in the Mediterranean Sea ecosystem: Insight from a coupled model. Journal of Marine Systems.
1090 https://doi.org/10.1016/j.jmarsys.2019.05.002, 2019.

1091

1092 D'Ortenzio, F., Antoine, D. and Marullo, S.: Satellite-driven modeling of the upper ocean mixed layer and air–sea CO2
1093 flux in the Mediterranean Sea. Deep Sea Research Part I: Oceanographic Research Papers, 55(4), pp.405-434, 2008.

1094

1095 D'Ortenzio, F. and D'Alcala, M.R.: On the trophic regimes of the Mediterranean Sea: a satellite analysis. Biogeosciences
1096 6 (2), 139-148, 2009.

1097

1098 Diffenbaugh, N. S., Pal, J. S., Giorgi, F., and Gao, X.: Heat stress intensification in the Mediterranean climate change
1099 hotspot. Geophys. Res. Lett. 34:GL030000. doi: 10.1029/2007GL030000, 2007.

1100
1101
1102 Dubois, C., Somot, S., Calmanti, S., Carillo, A., Déqué, M., Dell'Aquilla, A., Elizalde, A., Jacob, D., L'Hévéder, B.,Li,
1103 L., Oddo, P., Sannino, G., Scoccimarrio, E., Sevault, F.: Future projections of the surface heat and water budgets of the
1104 Mediterranean Sea in an ensemble of coupled atmosphere–ocean regional climate models.*Climate dynamics*, *39*(7), 1859-
1105 1884, 2012.

1106

1107   Fach, B. A., Orek, H., Yilmaz, E., Tezcan, D., Salihoglu, I., Salihoglu, B., and Latif, M. A.: Water Mass Variability and
1108   Levantine Intermediate Water Formation in the Eastern Mediterranean Between 2015 and 2017. *Journal of Geophysical*
1109   *Research: Oceans*, *126*(2), e2020JC016472., 2021.

1110

1111   Fedele, G., Mauri, E., Notarstefano, G., Poulain, P. M.: Characterization of the Atlantic Water and Levantine Intermediate
1112   Water in the Mediterranean Sea using Argo Float Data. *Ocean Science Discussions*, 1-41, 2021.

1113

1114   Foujols, M.-A., Lévy, M., Aumont, O., Madec, G.: OPA 8.1 Tracer Model Reference Manual. Institut Pierre Simon
1115   Laplace, pp. 39, 2000.

1116

1117   Gačić, M., Borzelli, G. L. E., Civitarese, G., Cardin, V., Yari, S.,Can internal processes sustain reversals of the ocean
1118   upper circulation? The Ionian Sea example,*Geophys. Res. Lett.*, 37, L09608, doi:10.1029/2010GL043216, 2010.

1119

1120   Galli, G., Lovato, T., Solidoro, C.: Marine Heat Waves Hazard 3D Maps and the Risk for Low Motility Organisms in a
1121   Warming Mediterranean Sea. Frontiers in Marine Science 4:136. doi: 10.3389/fmars.2017.00136, 2017.

1122

1123   Gazeau, F., Ridame, C., Van Wambeke, F., Alliouane, S., Stolpe, C., Irisson, J.-O., Marro, S., Grisoni, J.-M., De Liège,
1124   G., Nunige, S., Djaoudi, K., Pulido-Villena, E., Dinasquet, J., Obernosterer, I., Catala, P., and Guieu, C.: Impact of dust
1125   addition on Mediterranean plankton communities under present and future conditions of pH and temperature: an
1126   experimental overview, Biogeosciences, 18, 5011–5034, https://doi.org/10.5194/bg-18-5011-2021, 2021.

1127

1128   Giorgi, F: Climate change hot-spots. *Geophysical research letters*, *33*(8)2006

1129

1130   Giorgi, F, Lionello, P: Climate Change Projections for the Mediterranean Region. *Glob Planet Change* 63:90-104. doi:
1131   10.1016/jgloplacha200709005, 2008.

1132

1133   Goyet, C., Hassoun, A., Gemayel, E., Touratier, F., Abboud-Abi Saab, M. and Guglielmi, V.: Thermodynamic forecasts
1134   of the Mediterranean Sea acidification. Mediterranean Marine Science, 17(2), pp.508-518., 2016.

1135

1136   Gualdi, S., Somot, S., Li, L., Artale, V., Adani, M., Bellucci, A., Braun, A., Calmanti, S., Carillo, A., Dell'Aquila, A.,
1137   Déqué, M., Dubois, C., Elizalde, A., Harzallah, A, Jacob, D., L'Hévéder, B., May, W., Oddo, P., Ruti, P., Sanna, A.,
1138   Sannino, G., Scoccimarro, E.,Sevault, F., Navarra, A : The CIRCE simulations: Regional climate change projections with
1139   realistic representation of the Mediterranean sea. *Bulletin of the American Meteorological Society, 94*, 65-81.
1140   doi:10.1175/BAMS-D-11-00136.1, 2013.

1141

1142 Guyennon, A., Baklouti, M., Diaz, F., Palmieri, J., Beuvier, J., Lebaupin-Brossier, C., Arsouze, T., Béranger, K., Dutay,
1143 J.-C., and Moutin, T.: New insights into the organic carbon export in the Mediterranean Sea from 3-D modeling,
1144 Biogeosciences, 12, 7025–7046, https://doi.org/10.5194/bg-12-7025-2015, 2015.

1145

1146 Hassoun, A.E.R., Gemayel, E., Krasakopoulou, E., Goyet, C., Abboud-Abi Saab, M., Guglielmi, V., Touratier, F. and
1147 Falco, C., : Acidification of the Mediterranean Sea from anthropogenic carbon penetration. Deep Sea Research Part I:
1148 Oceanographic Research Papers, 102, pp.1-15, 2015.

1149

1150 Hassoun, A. E. R., Fakhri, M., Abboud-Abi Saab, M., Gemayel, E., and De Carlo, E. H: The carbonate system of the
1151 Eastern-most Mediterranean Sea, Levantine Sub-basin: Variations and drivers. *Deep Sea Research Part II: Topical*
1152 *Studies in Oceanography*, *164*, 54-73, 2019.

1153

1154 Hausfather, Zeke, Glen P. Peters: "Emissions-the 'business as usual' story is misleading." Nature 577.7792 : 618-620,
1155 2020.

1156

1157 Herrmann, M., Somot, S., Sevault, F., Estournel, C., and Déqué, M.: Modeling the deep convection in the northwestern
1158 Mediterranean Sea using an eddy-permitting and an eddy-resolving model: Case study of winter 1986–1987, J. Geophys.
1159 Res., 113, C04011, doi:10.1029/2006JC003991, 2008.

1160

1161 Herrmann, M., Diaz, F., Estournel, C., Marsaleix, P., Ulses, C.: Impact of atmospheric and oceanic interannual variability
1162 on the North Western Mediterranean Sea pelagic planktonic ecosystem and associated carbon cycle, *J. Geophys. Res.*
1163 *Oceans*, 118, 5792–5813, doi:10.1002/jgrc.20405, 2013.

1164

1165 Herrmann, M., Estournel, C., Adloff, F., and Diaz, F.: Impact of climate change on the northwestern Mediterranean Sea
1166 pelagic planktonic ecosystem and associated carbon cycle, J. Geophys. Res. Oceans, 119, 5815– 5836,
1167 doi:10.1002/2014JC010016, 2014.

1168 Howes, EL., Stemmann, L., Assailly, C, Irisson, JO, Dima, M, Bijma, J, Gattuso, JP : Pteropod time series from the North
1169 Western Mediterranean (1967-2003): impacts of pH and climate variability. Mar Ecol Prog Ser 531:193-206.
1170 https://doi.org/10.3354/meps11322, 2015.

1171

1172 Ibrahim, O., Mohamed, B., Nagy, H.: Spatial Variability and Trends of Marine Heat Waves in the Eastern Mediterranean
1173 Sea over 39 Years. *J. Mar. Sci. Eng. 9*, 643. https://doi.org/10.3390/jmse9060643, 2021.

1174

1175 IPCC AR5 Climate Change 2014: Synthesis Report. Contribution of Working Groups I, II and III to the Fifth Assessment
1176 Report of the Intergovernmental Panel on Climate Change, 2014.

1177 Keeling, R. F., Kortzinger A., and Gruber N.: Ocean Deoxygenation in a Warming World *Annual Review of Marine*
1178 *Science* 2: 199-229, 2010.

1179 Kwiatkowski, L., Torres, O., Bopp, L., Aumont, O., Chamberlain, M., Christian, J. R., Dunne, J. P., Gehlen, M., Ilyina,
1180 T., John, J. G., Lenton, A., Li, H., Lovenduski, N. S., Orr, J. C., Palmieri, J., Santana-Falcón, Y., Schwinger, J., Séférian,
1181 R., Stock, C. A., Tagliabue, A., Takano, Y., Tjiputra, J., Toyama, K., Tsujino, H., Watanabe, M., Yamamoto, A., Yool,
1182 A., and Ziehn, T.: Twenty-first century ocean warming, acidification, deoxygenation, and upper-ocean nutrient and
1183 primary production decline from CMIP6 model projections, Biogeosciences, 17, 3439–3470, https://doi.org/10.5194/bg-
1184 17-3439-2020, 2020.

1186 Lamon, L., Rizzi, J., Bonaduce, A. et al.: An ensemble of models for identifying climate change scenarios in the Gulf of
1187 Gabes, Tunisia Reg Environ Change 31. https://doi.org/10.1007/s10113-013-0430-x, 2014.

1190 Lazzari, P., Solidoro, C., Ibello, V., Salon, S., Teruzzi, A., Béranger, K., Colella, S., Crise, A.: Seasonal and inter-annual
1191 variability of plankton chlorophyll and primary production in the Mediterranean Sea: a modelling approach,
1192 Biogeosciences, 9, 217-233, doi:10.5194/bg-9-217-2012, 2012.

1194 Lazzari, P., Mattia,G., Solidoro, C., Salon,S., Crise,A., Zavatarelli,M., Oddo,P., Vichi M.,: The impacts of climate change
1195 and environmental management policies on the trophic regimes in the Mediterranean Sea: Scenario analyses Journal of
1196 Marine Systems Sea, 2014.

1198 Lazzari, P, Solidoro C., Salon S., Bolzon G.: Spatial variability of phosphate and nitrate in the Mediterranean Sea: A
1199 modeling approach Deep Sea Research Pages 39-52, 2016.

1201 Lavigne, H., D'Ortenzio, F., D'Alcalà, M. R., Claustre, H., Sauzede, R., and Gacic, M.: On the vertical distribution of the
1202 chlorophyll a concentration in the Mediterranean Sea: a basin-scale and seasonal approach. Biogeosciences, 12(16), 5021-
1203 5039, 2015.

1205 Lionello, P., Abrantes,F. Congedi,L., Dulac, F., Gacic,M.,Gomis,D., Goodess, C., Hoff,H. Kutiel,H., Luterbacher, J.,
1206 Planton,S. , Reale,M., Schröder, K., Struglia,M.V., Toreti, A.,Tsimplis, M.,Ulbrich, U., Xoplaki E.: Introduction:
1207 Mediterranean Climate: Background Information in Lionello P. (Ed.) The Climate of the Mediterranean Region. From
1208 the Past to the Future, Amsterdam: Elsevier (NETHERLANDS), XXXV-lXXX, ISBN:9780124160422, 2012.

1210 Lovato, T., Vichi, M., Oddo, P.: High-resolution simulations of Mediterranean Sea physical oceanography under current
1211 and scenario climate conditions: model description, assessment and scenario analysis. CMCC Research Paper,
1212 RP0207.2013, 2013.

1214 Macias, D., Stips, A., and Garcia-Gorriz, E.: The relevance of deep chlorophyll maximum in the open Mediterranean Sea
1215 evaluated through 3D hydrodynamic-biogeochemical coupled simulations. Ecological Modelling, 281, 26-37, 2014.

1216

1217 Macias, D. M., Garcia-Gorriz, E., and Stips, A.: Productivity changes in the Mediterranean Sea for the twenty-first century
1218 in response to changes in the regional atmospheric forcing. Frontiers in Marine Science, 2, 79, 2015.

1219

1220 Macias D., Garcia-Gorriz E., Stips A.: Deep winter convection and phytoplankton dynamics in the NW Mediterranean
1221 Sea under present climate and future (horizon 2030) scenarios. Sci. Rep. 22, 1–15. https://doi.org/10.1038/s41598-018-
1222 24965-0.2018, 2018.

1223

1224 Madec, G.: NEMO Ocean Engine. Note du Pôle de modélisation, No 27, Institut Pierre-Simon Laplace (IPSL), France,
1225 2008.

1226

1227 Mantziafou, A. and Lascaratos, A: An eddy resolving numerical study of the general circulation and deep-water formation
1228 in the Adriatic Sea, Deep Sea Res., Part I, 51(7), 251–292., 2004.

1229

1230 Mantziafou, A. and Lascaratos, A.: Deep-water formation in the Adriatic Sea: Interannual simulations for the years 1979-
1231 1999, Deep Sea Res., Part I, 55, 1403–1427, 2008.

1232

1233 Mathbout, S., Lopez-Bustins, J.A., Royé, D., Martin-Vide, J.: Mediterranean-Scale Drought: Regional Datasets for
1234 Exceptional Meteorological Drought Events during 1975–2019. *Atmosphere, 12*, 941.
1235 https://doi.org/10.3390/atmos12080941, 2021.

1236

1237 MedECC (2020) Climate and Environmental Change in the Mediterranean Basin – Current Situation and Risks for the
1238 Future. First Mediterranean Assessment Report [Cramer, W., Guiot, J., Marini, K. (eds.)] Union for the Mediterranean,
1239 Plan Bleu, UNEP/MAP, Marseille, France, 632pp., ISBN: 978-2-9577416-0-1, DOI: 10.5281/zenodo.4768833, 2020.

1240

1241 Myers, PG and Haines, K: Stability of the Mediterranean's thermohaline circulation under modified surface evaporative
1242 fluxes. J Geophys Res 107(C3):7-1-10, 2002.

1243

1244 Morel, A. and Gentili, B.: The dissolved yellow substance and the shades of blue in the Mediterranean Sea,
1245 Biogeosciences, 6, 2625–2636, https://doi.org/10.5194/bg-6-2625-2009, 2009.

1246

1247 Moullec, F., Barrier, N., Drira, S., Guilhaumon, F., Marsaleix, P., Somot, S., Ulses, C., Velez, L., Shin, Y. J.: An end-to-
1248 end model reveals losers and winners in a warming Mediterranean Sea. *Frontiers in Marine Science*, *6*, 345, 2019.

1249

1250 Moutin, T. and Raimbault, P.: Primary production, carbon export and nutrients availability in Western and Eastern
1251 Mediterranean Sea in early summer 1996 (MINOS cruise), J. Marine Syst.,33/34, 273–288, 2002.

1252

Moutin, T. and Prieur, L.: Influence of anticyclonic eddies on the Biogeochemistry from the Oligotrophic to the Ultraoligotrophic Mediterranean (BOUM cruise), Biogeosciences, 9, 3827–3855, https://doi.org/10.5194/bg-9-3827-2012, 2012.

Moss, R. H., Edmonds, J. A., Hibbard, K. A., Manning, M. R., Rose, S. K., Van Vuuren, D. P., Meehl, G. A.: The next generation of scenarios for climate change research and assessment. Nature, 463(7282), 747-756, 2010.

O'Connor, M. I., Gilbert, B., and Brown, C. J.: Theoretical predictions for how temperature affects the dynamics of interacting herbivores and plants. The American Naturalist, 178(5), 626-638, 2011.

O'Neill, B. C., Tebaldi, C., van Vuuren, D. P., Eyring, V., Friedlingstein, P., Hurtt, G., Knutti, R., Kriegler, E., Lamarque, J.-F., Lowe, J., Meehl, G. A., Moss, R., Riahi, K., and Sanderson, B. M.: The Scenario Model Intercomparison Project (ScenarioMIP) for CMIP6, Geosci. Model Dev., 9, 3461–3482, https://doi.org/10.5194/gmd-9-3461-2016, 2016.

Oddo, P., Adani, M., Pinardi, N., Fratianni, C., Tonani, M., and Pettenuzzo, D.: A nested Atlantic-Mediterranean Sea general circulation model for operational forecasting. Ocean Science, 5, 461–473. https://doi.org/10.5194/os-5-461-2009, 2009.

Pagès R., Baklouti, M., Barrier, N., Ayache, M., Sevault, F., Somot, S., and Moutin, T..: Projected Effects of Climate-Induced Changes in Hydrodynamics on the Biogeochemistry of the Mediterranean Sea Under the RCP 8.5 Regional Climate Scenario. Frontiers in Marine Science, 7, 957, 2020.

Planton, S., Lionello, P., Artale,V., Aznar, R., Carrillo, A., Colin,J., Congedi, L., Dubois, C., Elizalde, A.,Gualdi, S., Hertig, E., Jacobeit, J., Jordà, G., Li, L., Mariotti, A., Piani, C., Ruti,P., Sanchez-Gomez, E., Sannino, G., Sevault, F., Somot, S., TsimplisM.:The Climate of the Mediterranean Region in Future Climate in Lionello P. (Ed.) The Climate of the Mediterranean Region. From the Past to the Future, Amsterdam: Elsevier (NETHERLANDS), Projections 449-502, 2012.

Powley, H. R., Krom, M. D., and Van Cappellen, P.: Circulation and oxygen cycling in the Mediterranean Sea: Sensitivity to future climate change, *J. Geophys. Res. Oceans*, 121, 8230– 8247, doi:10.1002/2016JC012224, 2016.

Ramirez-Romero, E., Jordà, G., Amores, A., Kay, S., Segura-Noguera, M., Macias, DM., Maynou, F., Sabatés, A. and Catalán, IA.: Assessment of the Skill of Coupled Physical–Biogeochemical Models in the NW Mediterranean. Front. Mar. Sci. 7:497. doi: 10.3389/fmars.2020.00497, 2020.

1289   Reale, M., Giorgi, F., Solidoro, C., Di Biagio, V., Di Sante, F., Mariotti, L., Farneti, R., Sannino, G.: The Regional Earth
1290   System Model RegCM-ES: Evaluation of the Mediterranean climate and marine biogeochemistry. *Journal of Advances*
1291   *in Modeling Earth Systems*, 12, e2019MS001812. https://doi.org/10.1029/2019MS001812, 2020a.

1292

1293   Reale, M., Salon, S., Somot, S., Solidoro, C., Giorgi, F., Cossarini, G., Lazzari, P., Crise, A., Sevault, F.: Influence of
1294   large-scale atmospheric circulation patterns on nutrients dynamics in the Mediterranean Sea in the extended winter season
1295   (October-March) 1961-1999 *Climate Research* https://doi.org/10.3354/cr01620, 2020b.

1296

1297   Richon, C., Dutay, J.-C., Dulac, F., Wang, R., Balkanski, Y.: Modeling the biogeochemical impact of atmospheric
1298   phosphate deposition from desert dust and combustion sources to the Mediterranean Sea, Biogeosciences, 15, 2499–2524,
1299   https://doi.org/10.5194/bg-15-2499-2018, 2018.

1300

1301   Richon, C., Dutay, J.-C., Bopp, L., Le Vu, B., Orr, J. C., Somot, S., Dulac, F.: Biogeochemical response of the
1302   Mediterranean Sea to the transient SRES-A2 climate change scenario, Biogeosciences, 16, 135-165,
1303   https://doi.org/10.5194/bg-16-135-2019, 2019.

1304

1305   Salon, S., Cossarini, G., Bolzon, G., Feudale, L., Lazzari, P., Teruzzi, A., Solidoro, C., and Crise, A.: Novel metrics based
1306   on Biogeochemical Argo data to improve the model uncertainty evaluation of the CMEMS Mediterranean marine
1307   ecosystem forecasts, Ocean Sci., 15, 997–1022, https://doi.org/10.5194/os-15-997-2019, 2019.

1308

1309   Schroeder, K., Garcìa-Lafuente, J., Josey, SA, Artale, V., Nardelli, BB., Carrillo, A., Gačić, M., Gasparini, GP.,
1310   Herrmann, M., Lionello, P., Ludwig, W., Millot, C., Özsoy, E., Pisacane, G., Sánchez-Garrido, JC., Sannino, G.,
1311   Santoleri, R., Somot, S., Struglia, M., Stanev, E., Taupier-Letage, I., Tsimplis, MN., Vargas-Yáñez, M., Zervakis V.,
1312   Zodiatis, G.: Circulation of the Mediterranean Sea and its Variability. in P Lionello (ed.), *The Climate of the*
1313   *Mediterranean Region: From the Past to the Future.* Elsevier Inc., pp. 187-256. https://doi.org/10.1016/B978-0-12-
1314   416042-2.00003-3, 2012.

1315

1316   Scoccimarro, E., Gualdi,S., Bellucci, A., Sanna, A., Fogli, P.G., Manzini, E., Vichi, M., Oddo, P.,and Navarra, A.:
1317   Effects of Tropical Cyclones on Ocean Heat Transport in a High Resolution Coupled General Circulation Model. Journal
1318   of Climate, 24, 4368-4384, 2011.

1319

1320   Shepherd, J. G., Brewer, P. G., Oschlies, A., & Watson, A. J.: Ocean ventilation and deoxygenation in a warming world:
1321   introduction and overview. *Philosophical Transactions of the Royal Society A: Mathematical, Physical and Engineering*
1322   *Sciences*, *375*(2102), 20170240, 2017.

1323

1324   Simoncelli, S., Fratianni, C., Pinardi, N., Grandi, A., Drudi, M., Oddo, P., and Dobricic, S.: Mediterranean Sea Physical
1325   Reanalysis (CMEMS MED-Physics) [Data set]. Copernicus Monitoring Environment Marine Service (CMEMS).
1326   https://doi.org/10.25423/MEDSEA_REANALYSIS_PHYS_006_004, 2019.

1327

Siokou-Frangou, I., Christaki, U., Mazzocchi, M., Montresor, M., Ribera d'Alcala, M., Vaque, D., Zingone, A.: Plankton in the open Mediterranean sea: a review. Biogeosciences,7(5):1543-1586., 2010.

Sitz, L. E., Di Sante, F., Farneti, R., Fuentes-Franco, R., Coppola, E., Mariotti, L., Reale, M., Sannino, G., Barreiro, M., Nogherotto, R., Giuliani, G., Graffino, G., Solidoro, C., Cossarini, G., and Giorgi, F.: Description and evaluation of the Earth System Regional Climate Model (Reg CM-ES). Journal of Advances in Modeling Earth Systems, 9, 1863–1886. https://doi.org/10.1002/2017MS000933, 2017.

Solidoro, C., Cossarini, G., Lazzari, P., Galli, G., Bolzon, G., Somot, S., Sevault, F., Salon, S.: Modelling carbon budgets in the Mediterranean Sea ecosystem under contemporary and future climate. *Frontiers in Marine Sciences,* 2022.

Somot, S., Sevault, F., Déqué, M.: Transient climate change scenario simulation of the Mediterranean Sea for the 21st century using a high-resolution ocean circulation model. Climate Dynamics, Springer Verlag, 27 (7-8), pp.851-879. ff10.1007/s00382-006-0167-zff. ffhal-00195045f, 2006.

Somot, S., Houpert, L., Sevault, F., Testor, P., Bosse, A., Taupier-Letage, I, Bouin, M., Waldman, R., Cassou, C., Sanchez-Gomez, E., Durrieu de Madron, X., Adloff, F., Nabat, P., Herrmann, M.: Characterizing, modelling and understanding the climate variability of the deep water formation in the North-Western Mediterranean Sea. Climate Dynamics 51, 1179–1210. https://doi.org/10.1007/s00382-016-3295-0, 2018.

Soto-Navarro, J., Jordá, G., Amores, A., Cabos, W., Somot, S., Sevault, F., Macias, D., Djurdjevic V., Sannino G., Li, L., Sein D. : Evolution of Mediterranean Sea water properties under climate change scenarios in the Med-CORDEX ensemble, *Clim Dyn* 54, 2135–2165. https://doi.org/10.1007/s00382-019-05105-4, 2020.

Stöven, T. and Tanhua, T.: Ventilation of the Mediterranean Sea constrained by multiple transient tracer measurements, Ocean Sci., 10, 439–457, https://doi.org/10.5194/os-10-439-2014, 2014.

Taylor, K. E., Stouffer, R. J., and Meehl, G. A.: An Overview of CMIP5 and the Experiment Design, B. Am. Meteorol. Soc., 93, 485–498, https://doi.org/10.1175/BAMS-D-11-00094.1, 2012.

Teruzzi, A., Dobricic, S., Solidoro, C., Cossarini, G.: A 3D variational assimilation scheme in coupled transport biogeochemical models: Forecast of Mediterranean biogeochemical properties, Journal of Geophysical Research, doi:10.1002/2013JC009277, 2014.

Teruzzi, A., Bolzon, G., Salon, S., Lazzari, P., Solidoro, C., Cossarini, G.: Assimilation of coastal and open sea biogeochemical data to improve phytoplankton simulation in the Mediterranean Sea. Ocean Modelling, https://doi.org/10.1016/j.ocemod.2018.09.0072018, 2018.

1367 Teruzzi, A., Bolzon, G., Cossarini, G., Lazzari, P., Salon, S., Crise, A., and Solidoro, C.: Mediterranean Sea
1368 Biogeochemical Reanalysis (CMEMS MED-Biogeochemistry) [Data set]. Copernicus Monitoring Environment Marine
1369 Service (CMEMS). https://doi.org/10.25423/MEDSEA_REANALYSIS_BIO_006_008, 2019.

1370

1371 Teruzzi, A., Feudale, L., Bolzon, G., Lazzari, P., Salon, S., Di Biagio, V., Coidessa, G., and Cossarini, G.: Mediterranean
1372 Sea Biogeochemical Reanalysis (CMEMS MED-Biogeochemistry, MedBFM3 system) (Version 1) [Data set].
1373 Copernicus   Monitoring   Environment   Marine   Service   (CMEMS).
1374 https://doi.org/10.25423/CMCC/MEDSEA_MULTIYEAR_BGC_006_008_MEDBFM3, 2021.

1375

1376 Thingstad, T. F., Krom, MD, Mantoura, RF, Flaten, GA, Groom, S, Herut, B, Kress, N, Law, CS, Pasternak, A, Pitta, P,
1377 Psarra, S, Rassoulzadegan, F, Tanaka, T, Tselepides, A, Wassmann, P, Woodward, EM, Riser, CW, Zodiatis, G, Zohary,
1378 T. : Nature of phosphorus limitation in the ultraoligotrophic Eastern Mediterranean. *Science* 309.5737: 1068-1071, 2005.

1379

1380 Van Apeldoorn, D. and Bouwman, L.: SES land-based runoff and nutrient load data (1980-2000), Deliverable 4.6,
1381 http://www.perseus-net.eu/assets/media/PDF/deliverables/3321.6_Final.pdf, last access 05-02-2020, 2014.

1382

1383 Velaoras, D., Papadopoulos, V. P., Kontoyiannis, H., Cardin, V., & Civitarese, G. : . Water masses and hydrography
1384 during April and June 2016 in the cretan sea and cretan passage (Eastern Mediterranean Sea). *Deep Sea Research Part*
1385 *II: Topical Studies in Oceanography*, *164*, 25-40, 2019.

1386

1387 Vichi, M., Allen, J. I., Masina, S., and Hardman-Mountford, N. J.: The emergence of ocean biogeochemical provinces:
1388 A quantitative assessment and a diagnostic for model evaluation, *Global Biogeochem. Cycles*, 25, GB2005,
1389 doi:10.1029/2010GB003867, 2011.

1390

1391 Vichi, M., Cossarini, G., Gutierrez Mlot ,E., Lazzari, P., Lovato, T., Mattia, G., Masina, S., McKiver, W., Pinardi, N.,
1392 Solidoro, C., Zavatarelli, M., The Biogeochemical Flux Model (BFM): Equation Description and User Manual. BFM
1393 version 5 (BFM-V5). Release 1.0, BFM Report series N, 1. March 2013. CMCC, Bologna, Italy, http://bfm-
1394 community.eu, p. 87, 2015.

1395

1396 Waldman, R., Brüggemann, N., Bosse, A., Spall, M., Somot, S., and Sevault, F.: Overturning the Mediterranean
1397 thermohaline circulation. *Geophysical Research Letters*, 45, 8407– 8415. https://doi.org/10.1029/2018GL078502,2018.

1398

1399 Wimart-Rousseau, C., Lajaunie-Salla, K., Marrec, P., Wagener, T., Raimbault, P., Lagadec, V., Lafont, M., Garcia, N.,
1400 Diaz, F., Pinazo, C.,. Yohia, C., Garcia,F., Xueref-Remy, I., Blanc, P., Armengaud,A., and Lefèvre, D.: Temporal
1401 variability of the carbonate system and air-sea CO2 exchanges in a Mediterranean human-impacted coastal
1402 site. *Estuarine, Coastal and Shelf Science*, *236*, 106641, 2020.

1403

1404

1405 Wolf-Gladrow, D. A., Zeebe, R. E., Klaas, C., Körtzinger, A., and Dickson, A. G: Total alkalinity, the explicit
1406 conservative expression and its application to biogeochemical processes. Marine Chemistry, 106(1), 287-300, 2007.

1408 Zunino, S., Canu, D. M., Bandelj, V., and Solidoro, C.: Effects of ocean acidification on benthic organisms in the
1409 Mediterranean Sea under realistic climatic scenarios: a meta-analysis. *Regional Studies in Marine Science*, *10*, 86-96.,
1410 2017.

1412 Zunino, S., Canu, D. M., Zupo, V., and Solidoro, C.: Direct and indirect impacts of marine acidification on the ecosystem
1413 services provided by coralligenous reefs and seagrass systems. *Global Ecology and Conservation*, *18*, e00625, 2019.

1415 Zunino, S., Libralato, S., Melaku Canu, D., Prato G. and Solidoro C.: Impact of Ocean Acidification on Ecosystem
1416 Functioning   and   Services   in   Habitat-Forming   Species   and   Marine   Ecosystems. *Ecosystems*
1417 https://doi.org/10.1007/s10021-021-00601-3, 2021.